Electrochromic Properties of Tungsten Oxide Nanoparticles Films Prepared by the Filtration and Transfer Method

Youssef Mosaddeghian Golestani

A Thesis

In

The Department

Of

Physics

Presented in Partial Fulfillment of the Requirements

For the Degree of Master of Science in Physics at

Concordia University

Montreal, Quebec, Canada

March 2014

CONCORDIA UNIVERSITY
SCHOOL OF GRADUATE STUDIES

This is to certify that the thesis prepared

By: Youssef Mosaddeghian Golestani

Entitled: Electrochromic Properties of Tungsten Oxide Nanoparticles Films Prepared by the Filtration and Transfer Method

and submitted in partial fulfillment of the requirements for the degree of

Master of Science

Complies with the regulations of this University and meets the accepted standards with respect to originality and quality.

Signed by the final examining committee:

Prof. Laszlo Kalman Chair

Prof. Valter Zazubovich Examiner

Prof. Pablo Bianucci Examiner

Prof. Truong Vo-Van Supervisor

Approved by

Prof. Truong Vo-Van

Chair of the Department of Physics

March, 2014 Prof. Joanne Locke

Dean of Faculty

ABSTRACT

Electrochromic Properties of Tungsten Oxide Nanoparticles Films Prepared by the Filtration and Transfer Method

Youssef Mosaddeghian Golestani

Electrochromic tungsten oxide nanostructures were prepared from tungsten oxide nanoparticles for the first time by the filtration and transfer technique. This novel and facile method for film preparation presents many advantages that include the possibility to obtain nanoparticle films with various porosities and compositions. The films obtained in the present work exhibited indeed porous structures and were generally composed of a mixture of nanoparticles. When the amount of the nanoparticles in the suspensions increased, we observed thicker films with higher coverage densities. Films prepared at room temperature exhibited very good electrochromic properties. It was found that annealing at 500^{o}C increases the film stability and life time. Using cyclic voltammetry, fast diffusion behaviour (D of the order of 10^{-6} cm^2s^{-1}) for proton insertion/extraction has been observed. Moreover, fast switching response time (less than a second) during the bleaching process due to the rapid decay of the anodic current during chronoamperometry was also noted. The coloration efficiency for such devices was about 20 cm^2C^{-1}. The coloration of the films is associated with the number of color centers and depends on the number of inserted charges. However, we have shown that good optical reversibility does not necessarily need fast electrochemical kinetics. Finally, the effect of high applied potentials on the films was investigated, followed by an analysis of the electronic properties of the films.

Acknowledgments

First and foremost, I would like to sincerely express my deep gratitude to my thesis supervisor, Dr. Truong Vo-Van, who has always supported me throughout my study. I would like to acknowledge his advantageous guidance, continuous encouragement, effort and patience. I simply could not wish for a more enthusiast supervisor.

My special thanks go to our group members Drs. Simona Badilescu, Victor Stancovski, Mohammed Alsawafta and Hongjun Gao: I would like to thank Simona for helping me mostly with analytical writing and the analysis of electrochromic devices. She always put extra time to solve the problems encountered. I have never seen her answering no to any academic and support requests. I would like to thank Victor for the EIS measurements and his support for my thesis. I would also wish you, Mohammed, all the best for your upcoming career. I will not forget our productive conversations. Hongjun, for his part, has kindly initiated me to the filtration and transfer method used in this work.

Sincere regards are expressed to my thesis committee members, Drs. Laszlo Kalman, Valter Zazubovich and Pablo Bianucci, for their useful comments and advices.

I would also like to thank to my undergraduate teachers Dr. Mohammad Behshad Shafii, one of the most enlightened professors in the engineering departments, Dr. Ahmad Amjadi, a well-known name in the department of Physics in Sharif University of Technology and, of course, Mr. Abbas Aghakouchaki, the former National Men Basketball coach, who is still my number one athletic coach. I thank you all to supporting me up to this level!

The beautiful color of the objects would never be meaningful if there had not been a complementary concept of transparence. It is indeed the existence of such contrast that allows us to describe *color* and discover its extreme states. I would like to thank my parents in this regard. I could not have picked better ones.

Dedication

To my mom's transparent heart

Table of Contents

List of Tables

List of Figures

List of Symbols

A	(electrode) Area
Ag	silver
AgCl	silver chloride
ASR	Area specific resistance
c	Speed of light
C_0	Solution concentration
CA	Chronoamperometry
CC	Chronocoulometry
CV	Cyclic voltammetry
CE	Coloration efficiency
D	Diffusion coefficient
DOS	Density of states
DPV	Differential pulse voltammetry
e^-	Electron
E	Photon energy (chapter 2), Applied potential (chapter 4 and 5)
$E_{i=0}$	Open-circuit potential

EC	Electrochromic
ECD	Electrochromic device
EIS	Electrochemical Impedance Spectroscopy
FT	Filtration and transfer method
FTO	Fluorine doped tin oxide
GITT	Galvanostatic Intermittent Titration Technique
H^+	Hydrogen ion (proton)
H_2SO_4	Sulphuric acid
He	Helium
I	Current
I_0	Intensity of collected light
I_i	Intensity of incoming of light
i_p	Current peak
IPA	Isopropyl alcohol
IR	Infrared
ITO	Indium tin oxide
J	Current density

Li^+	Lithium ion
M	Alkali ion (chapter 2), Molar (chapter 3 and 5)
MV	Methyl viologen
n	Number of electrons
Na^+	Sodium ion
NPV	Normal pulse voltammetry
O	Oxygen
OD	Optical Density
Ox	Oxidized form
Q	Charge density (unless it is mentioned as charge)
Q_a	Anodic charge (density)
Q_{ca}	Cathodic charge (density)
R	Resistance
R&D	Research and Development
Red	Reduced form
SEM	Scanning electron microscope
SnO_2	Tin oxide

SWV	Square-wave voltammetry
t	time
T	Transmittance
TCO	Transparent conductive oxides
UV	Ultraviolet
VIS	Visible
W	Tungsten
WO_3	Tungsten trioxide (tungsten oxide)
x	Insertion coefficient
ν	Scan rate
η	Overpotential
ω	Frequency
λ	Wavelength
h	Plank's constant
ħ	Dirac's constant

1. Background and Motivation

1.1 Introduction

Since the last few decades, materials and material sciences have contributed greatly to our life style and its rapid change. Genesis of smart materials was a significant innovation in this direction and is considered as the third phase of the industrial revolution after electronics and computer revolutions [1]. Smartness in a material lies in the relationship between its appearance, properties and the energy applied to the material. Smart materials, unlike common ones, have more than one appearance according to their behaviour that varies with time due to an applied excitation [1].

Electrochromic materials are a category of smart materials that can change their optical properties (darken/lighten) in the presence of an electric potential [2]. Their ability to modulate solar radiation in different regions of the optical spectrum and their controlled functionality have been a considerable attraction for both academia and the market. They can be a basis for application in optical devices to control solar transmission or absorbance. Based on a recent report from Lawrence Berkeley National Laboratory, almost a quarter of the total energy in US is spent on lighting, heating and cooling the buildings [3]. Electrochromic devices can be therefore regarded as green and novel energy efficient substitutes in order to reduce the electrical consumption needed for air conditioners during the summer and a replacement for thermal windows during the winter time. One can also refer to antiglare automobile rear-view mirrors, displays, automobile

sunroofs and sensors as other remarkable examples of application of electrochromic materials [4] [5] [6] [7].

Among inorganic materials, tungsten oxide would be the most versatile material that has been extensively studied so far [8] [9]. High functionality and coloration efficiency, high contrast, overall chemical stability and life time have made tungsten oxide the first candidate for practical applications [10]. Tungsten oxide based devices exhibit a deep blue coloration and have the ability to stay colored for hours after the removal of the electric potential (electrochromic memory).

1.2 Background of Present Study

Different methods have been proposed to deposit the electrochromic films. The morphology of such films depends of the preparation technique and could be either amorphous or polycrystalline, or a mixture of both [11]. Common methods include (but are not limited to) physical techniques (evaporation and sputtering), chemical techniques (sol-gel, spray pyrolysis, and thermal oxidation) and electrochemical techniques (electrodeposition and anodization) [9].

Studies in particular of porous or nanostructured electrochromic films present a new facet to be explored for faster response time and better coloration efficiency. Recent works in such direction can be cited, using for example, the doctor blade method [12] [13]. Tungsten oxide, as the most promising candidate, has also kept its evolutionary pace with the recent development of various techniques to produce films with nanostructures of this

material [2] [14] [15]. Nanostructures of the electrochromic films largely affect the coloration process and it has been shown that enhanced coloration kinetics can be achieved [16]. The nanostructures of the films not only increase the surface area and ion insertion kinetics, but also reduce the material cost in large-area applications [2].

The operation of conventional electrochromic devices depends on the double injection of small positive ions (such as H^+, Li^+ and Na^+) and electrons in the host matrix of multivalent metal oxides, with positive ion insertion required to satisfy charge neutrality [9] [17] [18] [19] [20] [21]. Due to the higher diffusion behaviour of H^+, which is ten times larger than of other ions, devices working with a proton based electrolyte (such as aqueous H_2SO_4) are preferable for fast electrochromic applications [2]. Proton insertion, on the other hand, can result in degradation of electrochromic films. Thus, adapting of the device to the application has to be considered.

1.3 Contribution of this Work

Nanostructured tungsten oxide films were mostly prepared by methods involving high vacuum systems (e.g., sputtering). In order to avoid these costly techniques and to exploit the fact that it is now possible to synthesize nanoparticles of tungsten oxide, we propose an original method for preparing electrochromic films from nanoparticles. The method is based on the filtration and transfer (FT) originally developed for the fabrication of transparent thin films of carbon nanotubes [22] and is proven to be versatile, presenting many advantages. As far as we know, this is the first time that nanostructured electrochromic films are prepared in this way.

Firstly, a homogenous suspension of tungsten oxide nanoparticles is obtained by dispersing nano-powder of tungsten oxide, particle size in range of 50 – 100 nm, in a solution with a given proportion of particles. The suspension is then passed through a filter membrane with a small pore size as compared to the diameter of nanoparticles. The amount of deposited particles and the deposition rate are controlled by the concentration of the suspension and the vacuum pump pressure. Finally, the deposited film is transferred onto substrates coated with transparent indium tin oxide (ITO) films for study. Besides being a cost-effective, simple and yet very versatile method, the FT technique can be easily upscaled for production of large-area samples. Samples prepared in this way are found to be fairly homogeneous and their nanostructures can be adjusted according to experimental conditions.

In order to investigate the electrochromic properties of tungsten oxide nanoparticle films, we have examined suspensions with different amounts of nanoparticles which gave rise to formation of amorphous films. Up to now, amorphous tungsten oxide films have demonstrated the highest performance and efficiency [2]. These films, however, show a high rate of dissolution in acidic electrolytes and for this reason, the fabrication of other forms such as crystalline or polycrystalline films was also proposed [2]. We have subjected some samples to a thermal treatment in order to increase their crystallinity [23]. SEM images showed that nanoparticles in these films tend to aggregate at higher temperatures.

Two main electrochemical measurements (cyclic voltammetry and chronoamperometry) and their corresponding optical modulations were then utilized to describe the

electrochromic process. The voltammograms showed fast kinetics and the obtained diffusion coefficients of protons were in the range of 5.62×10^{-6} to 1.17×10^{-5} cm^2s^{-1}. This value was however lower (2.29×10^{-6} cm^2s^{-1}) for samples annealed at 500°C. Scanning at 5 mV/s, the optical modulation at λ_{max} reached 60%. During the chronoamperometry measurements, we observed a fast switching response time for the bleaching process (less than a second) and a maximum of 21.15 cm^2C^{-1} for coloration efficiency.

The optical properties of the films were equally studied and the transmittance of the colored films was found to be strongly dependent on the inserted protons [13].

2. Fundamentals of Electrochromism

2.1 Electrochromism

Electrochromism is the reversible change in the optical properties of a material when it becomes electrochemically reduced (electron uptake) or oxidized (electron release) [24]. Materials have been traditionally considered electrochromic when they exhibit changes in their distinct visible color, ranging between a transparent (bleached) state and a colored (opaque) state or between two colored states. In some cases there are more than two oxidation states and the material might exhibit several colors, according to the current oxidation state (polyelectrochromic materials [25]). Nowadays, the practical definition of electrochromism has been extended to include materials and devices used for the optical modulation of radiation in the near infrared as well as at microwave wavelengths. The term "-chromism" is, therefore, evaluated by the response by an adequate detector designed for these wavelengths [11] [26].

2.2 Electrochromic Materials

As suggested by Chang et al. [27] and more recently by Mortimer [11], we can sort electrochromic materials into three types based on their solubility of their oxidation state. For a given electrolyte solution, type I electrochromic materials are soluble in both their oxidation states. An example is methyl viologen (MV). Type II electrochromic materials are those that are soluble in one oxidation state but precipitate around one electrode while

electron transfer takes place. Heptyl viologen is a type II electrochromic material. Type III electrochromic materials are in solid forms in both or all oxidation states. Examples of this type of materials are tungsten oxide and Prussian blue. Systems based on type III materials are generally studied as thin films.

In cases of types II and III, once the corresponding oxidation state has been reached to for a new electrochromic state, the material can retain the color without any additional injection of charge. This property is called “optical memory” or simply “memory effect”. The higher the memory effect, the longer the electrochromic material can stay colored. For type I, however, the new soluble state diffuses away from the electrode until the whole solution is electrolyzed. In this case, it is necessary to keep the potential constant until saturation occurs [11].

Electrochromic materials can be found in a variety of materials. Inorganic materials are a large fraction of electrochromic materials. The oxides of the following metals have been shown to be electrochromic: cerium, chromium, cobalt, copper, iridium, iron, manganese, molybdenum, nickel, niobium, palladium, praseodymium, rhodium, ruthenium, tantalum, titanium, tungsten and vanadium [28]. Among these, oxides of iridium, molybdenum, nicked, titanium and tungsten exhibit high electrochromism [29]. Electrochromic properties can also be found in a number of organic materials. Materials such as the viologens, conducting polymers, metallopolymers and metallophthalocyanines have been shown to exhibit highly electrochromic behaviour [30].

2.3 Electrochemical Reaction and Coloration

An electroactive species can electrochemically gain electron(s) and undergo reduction reaction, Equation 2.1, or it can release electron(s), i.e. oxidation, the reverse of Equation 2.1.

$$\text{Oxidized form, O} + \text{electron(s)} \rightarrow \text{reduced form, R} \qquad (2.1)$$

These reactions take place at an electrode which is basically a metal or other conductor and is in contact with the forms O and R of the electroactive material via external connections (half-cell). In electrochromism, specifically, this electrode is a thin film of an adequate conductive semiconductor coated on glass substrate [28]. Furthermore, in the following section it will be mentioned that any electrode in an electrochemical system must be accompanied by a secondary passive electrode in order to allow the current flow through the system- the flow of those electrons as described by Equation 2.1 (full-cell).

White light comprises the wavelengths of all different colors. The human eye can detect wavelengths between 400-750 nm. Color observed is in fact the color complementary to that corresponding to the wavelength absorbed. Thus, for example, we can see the color blue because the material absorbs the red part. When a photon having energy '*E'* is absorbed by the color centers (also called chromophore [28]) of the material, it enables electrons to be promoted to an energy level which is higher than its initial level by a magnitude of *E* (allowed transitions). According Plank's relationship, expressed by Equation 2.2, the wavelength of the light absorbed is related to the magnitude of the energy gap between these levels:

$$E = \hbar\omega = hc/\lambda \tag{2.2}$$

where c is speed of light, ω and λ are the frequency and wavelength of light, respectively. h and ħ are the Plank and Dirac constants, respectively. The magnitude of E therefore relates to the color of the incoming photon.

During the reduction (or oxidization), the reaction leaves the electroactive species with the different number of electrons after the electron transfer in Equation 2.1 (or its reverse). These different oxidation states will necessarily exhibit different electronic structures and hence will require different transitional energy E for electron promotion between its allowed levels. We can therefore conclude that any material will change its absorption band when undergoes a reduction (or oxidation) reaction in Equation 2.1. In most cases in our routine life, this change is either very small or falls outside the visible range and cannot be observed by the naked eye.

Based on the redox sense, electrochromic materials are categorized in two groups. A first group changes their color under reduction reaction. These materials are colorless in oxidized state and colored in the reduced form (cathodically coloring materials). Oxides of niobium, titanium and tungsten are among this group. A second group of materials are those in which coloration is a result of oxidation such as iridium oxide and Prussian blue (anodically coloring materials). The devices built on these materials are called cathodic and anodic devices respectively.

2.4 Multi-Layer Device Assembly

Figure 2.1 shows the basic elements of an ideal electrochromic device which are two electronically conductive transparent electrodes which are coated onto the glass substrate, each at one side of the electrochromic device, an electrochromically active working electrode, an electrolyte (or ion conductor) and a secondary charge-balancing counter electrochromic electrode.

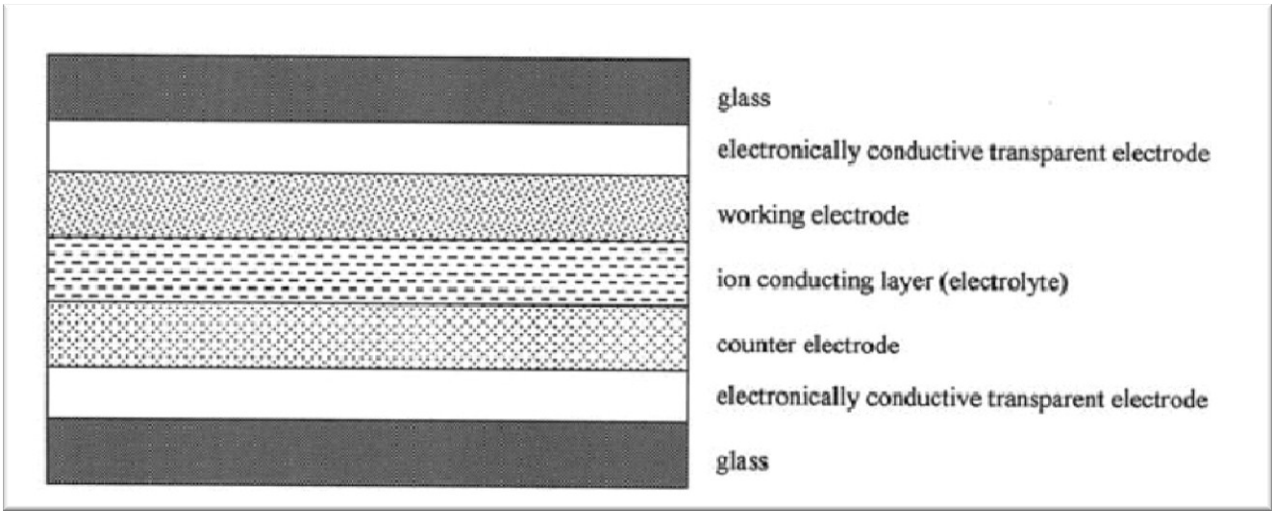

Figure 2.1: Schematic design of an ideal multi-layer electrochromic device. The device can be assumed as a rechargeable electrochemical cell in which coloration/bleaching is taking place by charging/discharging of an electrical potential (adapted from [24]).

A working electrode is in contact with the electrolyte which is conductive to a specific type of ion. On the other side, the electrolyte is in contact with the counter electrode. The counter electrochromic electrode should have complementary optical properties to the working one, i.e. coloration by anodic reaction if the working electrode is cathodic or vice versa. In other words, both should be colored at the same time, but not necessarily at

the same rate. In an absorptive/transmissive devise, the existence of the secondary electrode provides enhancement of the color/bleach contrast [11].

In a simpler case, the counter electrochromic electrode can be substituted with a non-electrochromic material (called ion storage) while maintaining its electrochemical performance. An electric field can force the ions into the working electrode from the ion storage and through the electrolyte. This is usually done by applying a small amount of voltage. In order to preserve charge neutrality electrons are simultaneously injected into the working electrode from the conductive transparent electrode. When the applied voltage is reversed, the ions are extracted from the film and return into the ion storage again. Likewise for electrons, reversed voltage implies electron to leave the film via the substrate. The electrochromic material is then returned to its initial state. This sandwich configuration is normally carried out in an electrochemical cell and allows the reversible reduction/oxidation reaction to cycle between the working and counter electrodes with injection/extraction of electrons and ions.

2.4.1 Electrochromic Layer

The working electrode is the optically active material in the electrochromic device and is (preferably) a thin film [31] and is deposited on the conductive transparent substrate. Such thin films could be either amorphous or polycrystalline, or a mixture of both. The morphology of the films depends significantly of the preparation of the oxide films [11]. Common techniques are physical techniques (evaporation and sputtering), chemical techniques (vapor deposition, sol-gel, spray pyrolysis, and thermal oxidation) and electrochemical techniques (electrodeposition and anodization) [9].

Materials that are initially colorless and can be chemically or electrochemically reduced to a non-stoichiometric oxidation state with an intense electronic absorption are considered good candidates for practical applications. However, other metal oxides with lower colorability are generally used as the complementary material in the counter electrode [11].

2.4.2 Optically Transparent Electrodes

The transparent conductor terminal connects the heart of the electrochromic device to an external power source and needs to show a low resistivity while maintaining transparency. It is very common to use a thin film of an oxide, one can refer to as transparent conductive oxides (TCOs). Tin oxide (SnO_2), fluorine doped tin oxide (FTO) and tin doped indium oxide (In_2O_3: Sn, commercially named ITO) are the most widely used TCOs so far [32]. For practical use, a thin film of a TCO is coated onto a transparent substrate such as glass or a flexible polyester foil. One of the transparent conductors is connected to the working electrochromic electrode and the other one is connected to the counter electrode.

2.4.3 Electrolyte

The electrolyte between the two electrodes must have a high conductivity and, ideally, should have zero electronic conductivity to ensure that after ion insertion the electrons neutralize the film from an outside source and do not influence the ionic current inside the electrolyte. In type I and II devices, the electrochromic material is dissolved in an aqueous or organic solvent electrolyte. In type III systems, on the other hand, the

electrolyte contains no electrochromic species but has two important roles. First, it ensures that during the coloration and bleaching sufficient counter-ions enter and leave the solid electrochromic layer to preserve electroneutrality. Second, it should be responsible for the conduction between the electrodes at the sides of the device [11].

The choice of electrolyte depends on the electrochromic material and its structure. Another important (but not critical) property of a good electrolyte would be a high quality of the interface between the electrolyte and the electrochromic layer. This ensures that there is a good ionic contact at the interface; however, this property becomes more significant when device assembly comes to an R&D level. For device fabrication it is more desirable to work with a solid or gel electrolyte. In the case of tungsten oxide, the electrochromic material exhibits good electrochemical performance in acidic electrolytes such as sulfuric acid.

2.4.4 Tungsten Oxide Electrochromic Device

One of the most widely studied electrochromic material is tungsten oxide. It is a cathodically coloring material and coloration occurs upon insertion of small ions such as proton and alkali metal ions like lithium and potassium. Figure 2.2 shows the schematic of the electrochemical reaction for tungsten oxide in an electrolyte which is conductive to protons [33]. When an electric potential is applied between the conductive transparent terminals protons and electrons follow into the tungsten oxide matrix and reduce it. Protons are inserting from the electrolyte and electrons insert into the side terminal which is in contact with the other side of electrochromic layer. When the applied voltage is

reversed, the protons and electrons are extracted from the film and return into the ion storage again.

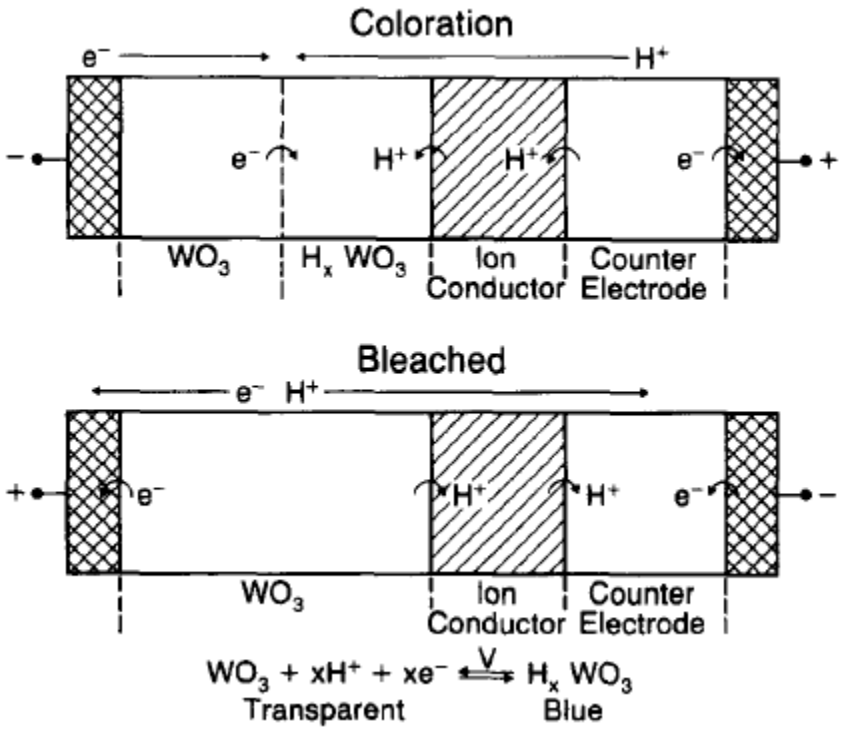

Figure 2.2: Drawing of the coloration and bleaching process of tungsten oxide in the electrochemical cell. Injection of protons and electrons cause formation of tungsten bronze (colored state, top), when the applied potential is reversed protons and electrons are ejected from tungsten bronze to re-form the initial tungsten oxide (transparent state, bottom), (adapted from [33]).

2.5 Electronic Structure of Tungsten Oxide

Electronic structure indicates how light interacts with the material [34] and so do the electrochromic properties. Thus in order to understand the coloration in tungsten oxide, electronic structure of tungsten in both oxide and reduced forms need to be understood.

The W-O bonds in tungsten oxide are more ionic compared to the covalence contribution and tungsten oxide can be regarded as being composed of W^{6+} and O^{2-} ions [9]. In general, tungsten oxide can be found in a large variety of crystal and disordered structural forms. It has been reported that tungsten oxide exhibits a stable monoclinic and hexagonal crystalline structure at room temperature [9] [35]. The reduced symmetry forms can occur due to the lattice variations of W-O and W-O-W bond length and the bond angle which is a result of deformation of its initial structure and can be a result of the donor concentration during the formation of the oxide or the annealing temperature. This deformation is a characteristic of all tungsten oxides [36] [37] [38] [39]. Basic building blocks and binding structure can be assumed for amorphous tungsten oxide as well.

Monoclinic and more complex structural forms of tungsten oxide require larger unit cells giving rise to more complex computations since W-W, O-O and W-O hybridization wave functions overlap in larger area. Surprisingly, one can consider a simplified cubic structure in order to investigate the general electronic band structure of tungsten oxide while maintaining overall comprehensive electronic features. Cubic structure is more likely to provide insights into the electronic structure in real tungsten oxide form. Presence of WO_6 octahedra in various corner-sharing or edge-sharing configurations is the dominant factor in controlling electronic properties and would legitimize the use of the simplification [40] [41] [42]. Figure 2.3 represents the cubic structure of tungsten oxide with the corner-sharing octahedra.

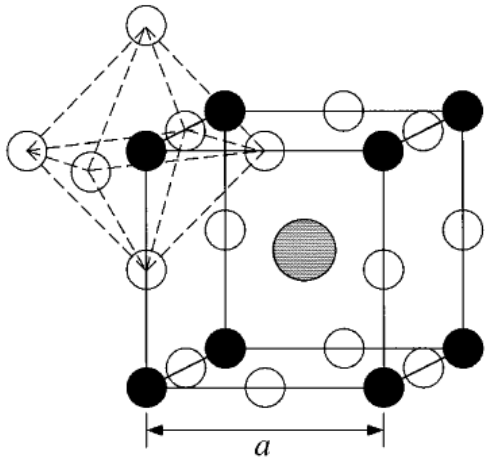

Figure 2.3: Approximation of monoclinic structure. Schematic cubic structure of tungsten oxide with solid and empty circles as tungsten and oxygen atoms respectively. Dashed circle in the middle is the inserted ion. The lattice constant 'a' is defined and octahedron is built up by six atoms of oxygen surrounding a tungsten atom (adapted from [40]).

Since the tungsten d states in tungsten atoms, [W] = [Xe] $4f^{14}5d^{4}6s^{2}$, are about 5 eV higher than oxygen p states in oxygen atom, [He] $2s^{2}2p^{4}$, it is more likely that the six tungsten valence electrons are transferred to the three oxygen p bands during the formation of tungsten oxide. The bandwidth is small enough to from a semiconductor with oxygen p states below the band gap and tungsten d states above. Figure 2.4 shows the density of states (DOS) curve for cubic structure of tungsten oxide.

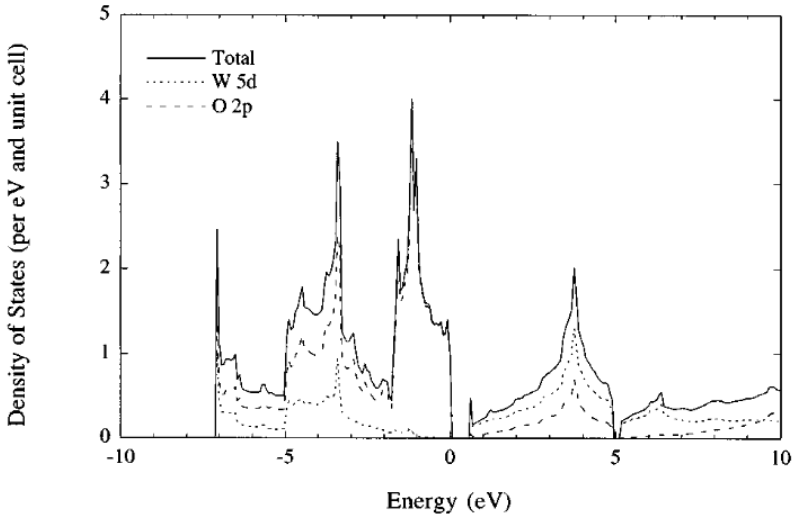

Figure 2.4: Density of states for cubic tungsten oxide, 2p orbital of oxygen and 5d orbitals of tungsten. At energies below zero all states found to be filled and empty states are above zero. Fermi energy, that is not shown here, is situated inside the band gap (adapted from [40]).

Tungsten bronze is formed (during the reduction reaction) when alkali metal ions such as lithium, sodium and potassium intercalate into a host matrix of tungsten oxide and in a position in the center of the unit cell. Hydrogen behaves differently from other ions and it becomes localized near an oxygen site in order to form a hydroxide unit [43]. Although the position of the intercalated ion in the matrix would change the representation of the unit cell, it has been shown that the electronic band structure does not vary significantly between hydrogen and other alkali metal ions [40].

Ipso facto, in the M_xWO_3 perovskite structure of tungsten oxide, there are x vacant sites within a molecule of tungsten oxide. The quantity of these sites highly depends on the oxygen vacancy concentration in WO_3 and therefore on the preparation method. Some of these sites are not active at the beginning of the electrochemical experiment and the

inserted ions irreversibly reside at these sites. These sites may later release the (trapped) ions as the electrochemical reaction proceeds. More specifically, the inserted protons have the chance to be localized at reversible sites or at irreversible trap sites initially at WO_3-electrolyte interface to form hydroxyl unit in W-OH for a short time to have stronger binding which can be released later [44] [45]. Schlotter et al. [46] and Yoskiike et al. [47] have reported a similar prediction for electrochromic devices based on tungsten oxide working with lithium ions.

2.6 Electrochromism in WO_3

In the case of tungsten oxide, thin film of tungsten oxide with the tungsten sites in the oxidation state W^{VI} is colorless or pale yellow. During the electrochemical reduction, Equation 2.3, W^{V} sites are formed and exhibit electrochromism:

$$WO_3 + xM^+ + xe^- \rightarrow M_xW^{VI}{}_{1-x}W^{V}{}_xO_3 \qquad (2.3)$$

(transparent) (colored)

where M is the metal ion such as hydrogen, lithium or sodium. The fractional number of sites which are reduced in the tungsten oxide is equal to *x* and is called insertion factor. At low values of *x* films exhibits a reversible blue color caused by the intervalence charge transfer (IVCT) between adjacent W^{V} and W^{VI} during the photon absorption as follows [48] [49]:

$$W^{VI}{}_{(a)} + W^{V}{}_{(b)} + h\nu \rightarrow W^{VI}{}_{(b)} + W^{V}{}_{(a)} \qquad (2.4)$$

At higher values of *x,* the insertion of ions irreversibly forms the metallic tungsten bronze which is red or golden [11]. For low charge levels the coloration is directly proportional to the charge injected; however, as the coloration proceeds an increasing amount of charge is needed to obtain a certain increase in optical modulation [50]. The model is phenomenologically relating the optical absorption in tungsten oxide to the transition between different charge states of W ions (W^{VI}, W^{V}). This is a general model and can be extended to further reduced forms of tungsten sites including W^{VI} and charge transfer has been proposed between all these sites.

Finally, it is still left as a challenge to find a comprehensive accepted mechanism for coloration of tungsten oxide in thin films of amorphous and crystalline owing to the many contradictions that still exist in the experimental results. Beside Deb's original model [51], there are four other common mechanisms: i) absorption by polaron; ii) interband excitations; iii) transitions from the valence band to split off the W^{V} state, and iv) IVCT which was briefly described above [11].

3. Experimental

The detailed procedure used for the preparation and the experimental setup are presented is this chapter.

The method for preparing electrochromic nanoparticle thin films is based on the filtration and transfer method first developed by Wu et al. [22] for deposition of carbon nanotube thin films. We have adapted it to the preparation of our thin films and found that it presents many advantages that include:

1. The possibility to work with nanoparticles of any size or type of electrochromic material
2. The possibility to control different important parameters such as the packing factor and film porosity by varying the particle concentration
3. The possibility to work with mixtures of different types of nanoparticles to tailor the sample optical properties
4. The simplicity and cost-efficient nature of the method involved

In our work, tungsten oxide nano-powders were firstly dispersed in a given solution, in order to produce a homogenous suspension. Particles were then transferred onto filter papers followed by a transfer deposition on a substrate.

Samples are identified, based on the amount of nanoparticles used to prepare the filters and the thermal treatment involved.

3.1 Substrate Preparation

Indium tin oxide (ITO) is used as the transparent conductive oxide (TCO) in this work. ITO is coated on a polished soda lime float glass from Colorado Concept Coatings, LLC. The coating sheet resistance of ITO was 15 Ω/sq. The transmittance of the ITO-glass in the visible and near infrared region is shown in the Figure 3.1.

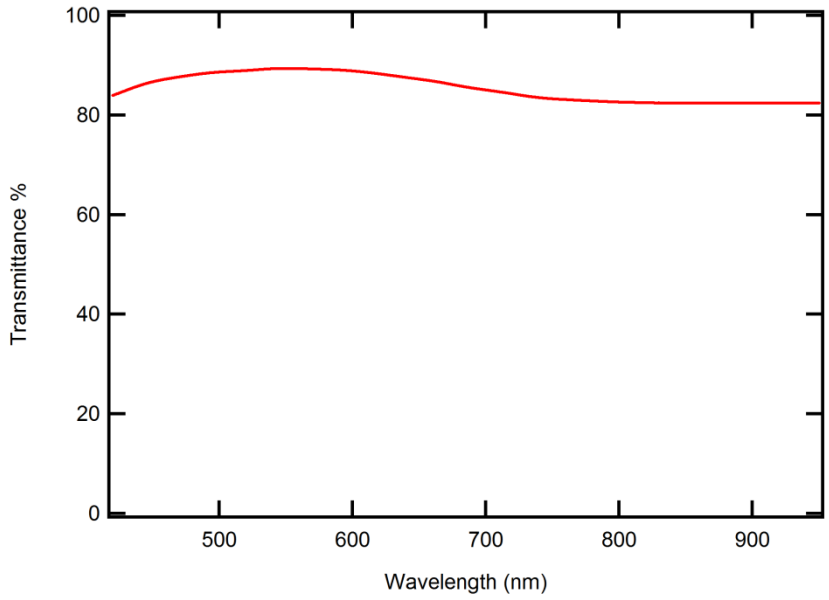

Figure 3.1: Transmittance of the ITO-glass in the visible and near infrared region

Large ITO-glass sheet was cut into smaller pieces to be used as substrates for experiments. The substrates were cleaned as follows:

1) Both sides of the substrates were washed with laboratory soap and deionized water to remove dust.
2) Acetone was used to remove chemical compounds from both sides of the substrate.

3) Isopropyl alcohol (IPA) was used to remove the acetone from both sides of substrate.
4) Samples were placed in an inclined position to dry.

3.2 Suspension Preparation

In order to prepare a homogenous suspension of tungsten oxide particles, a nano-powder of tungsten oxide, nanoparticles (purity: 99.5%, particle size in the range of 50 - 100 nm) supplied by SkySpring Nanomaterials Inc. (Figure 3.2), was dispersed in deionized water and methanol, in a 50%-50% proportion. The mixture was ultrasonicated in Branson 1510 ultrasonic cleaner for 30 minutes. The suspensions prepared with this process show high homogeneity as shown in Figure 3.3.

Figure 3.2: Yellowish nano-powder of tungsten oxide

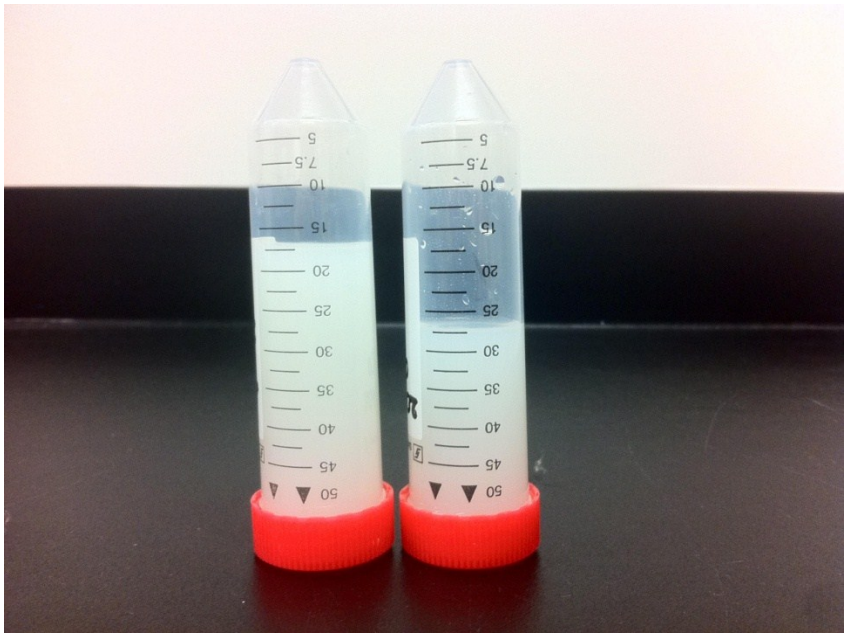

Figure 3.3: Suspension of tungsten oxide nano-powders in a mixture of deionized water and methanol

3.3 Filtration Technique

The suspension was filtered through a 0.05 μm pore size and 47 mm diameter mixed cellulose membrane, from Millipore Inc. using a Gast vacuum pump, DOA-P704. Generally speaking, vacuum filtration is a technique to separate a suspended solid product from its solution mixture. The filtration technique process for this work is as follows

1) The filter paper is kept in a deionized water bath for 5 minutes.
2) The Buchner funnel is fastened on the top of the vacuum flask.
3) The porcelain perforated plate is washed with deionized water and placed on top of Buchner funnel as shown in Figure 3.4.

4) The filter paper is removed from the bath and placed on top of the porcelain plate.
5) The glass funnel is placed on top of the filter paper and is clamped tightly to prevent leaking during the process.
6) The nozzle of the vacuum flask is connected to the vacuum source with a rubber as shown in Figure 3.5.
7) 300 ml of deionized water is poured in the funnel to decrease the depositing rate in step 8 and ensure the uniformity of deposition.
8) The prepared suspension is poured drop by drop from the top of the funnel with a plastic pipette in order to transfer it onto the funnel.
9) The vacuum source is turned on. The valve was set to produce a 0.2 bar pressure difference.

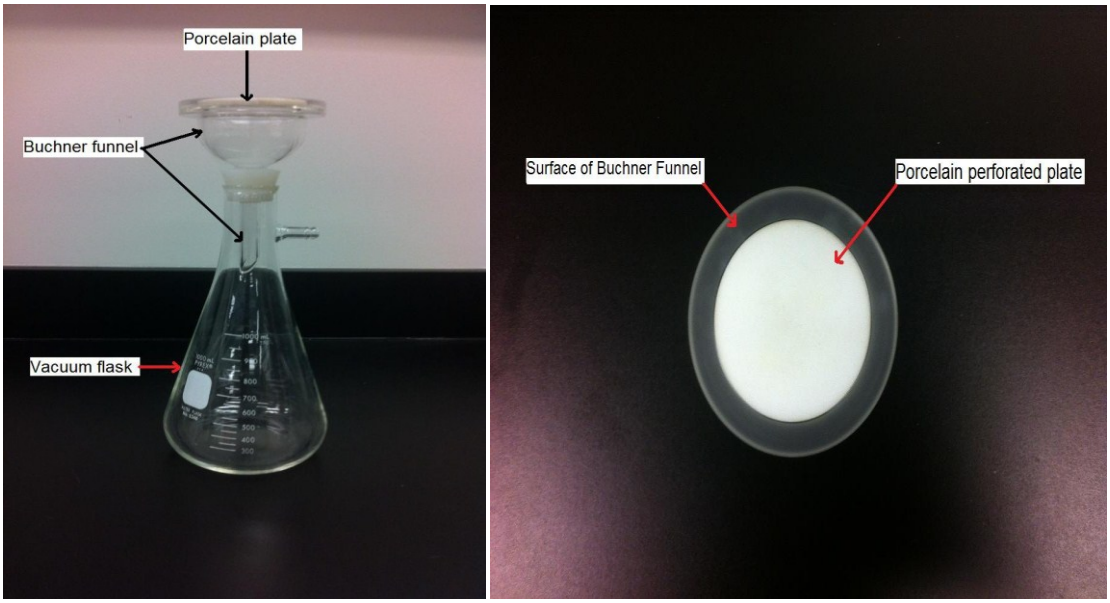

Figure 3.4: Configuration of the vacuum flask, the Buchner funnel and the porcelain plate: front view, left and top view, right; Steps 2 and 3

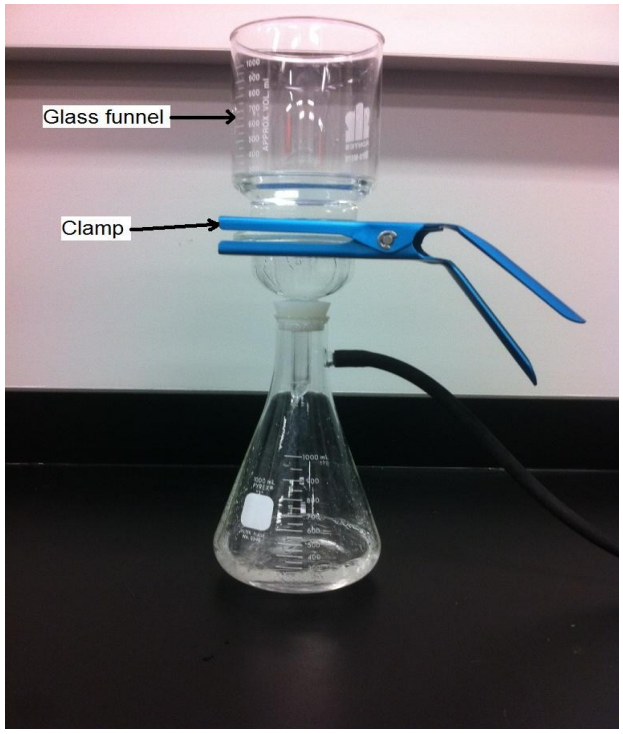

Figure 3.5: Filtration technique: the rubber tube is connected to the vacuum source. The pressure gradient between the funnel and the vacuum flask removes the solution from the funnel.

The vacuum source produces a pressure gradient between the funnel and the inside of the vacuum flask. This helps to facilitate filtering of the suspension. The solution passes through the filter paper and porcelain plate while leaving the solid particles on the filter paper. Tungsten oxide nanoparticles are therefore trapped by the filter paper and the tungsten oxide-free solution is drawn through the funnel into the flask. Filtration time depends on the total volume of the solutions at steps 7 and 8 and also the vacuum pressure value at step 9. For values mentioned for this work, the filtration process takes about 30 minutes to filter 40 ml of tungsten oxide suspension.

The filters were finally taken out and hung for 1 hour to dry (Figure 3.6).

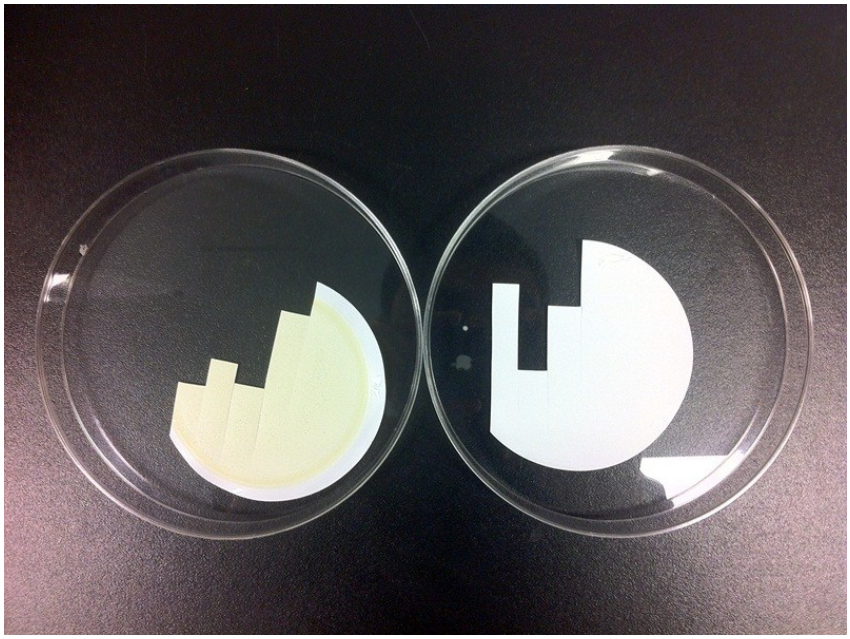

Figure 3.6: Filters with different amounts of tungsten oxide: higher (left) and lower (right)

3.4 Deposition Process

In order to transfer the tungsten oxide from the filter onto the substrates, the filters were cut into smaller pieces. Each piece was placed on the ITO-glass substrate in such a way that the side of the filter deposited with films faced the ITO side of substrate. One drop of 1,2-Dichlorobenzene (ODCB) was seeped at the interface to make the films adhere to ITO. Samples were placed horizontally in an acetone bath for 30 minutes. The filter paper, which is organic based cellulose, dissolves in the acetone. In order to remove the filters completely, the samples were tilted in the acetone bath for another 30 minutes so that the filter sediment is deposited in the bath. The process is shown in Figure 3.7. Finally, the samples were washed with deionized water.

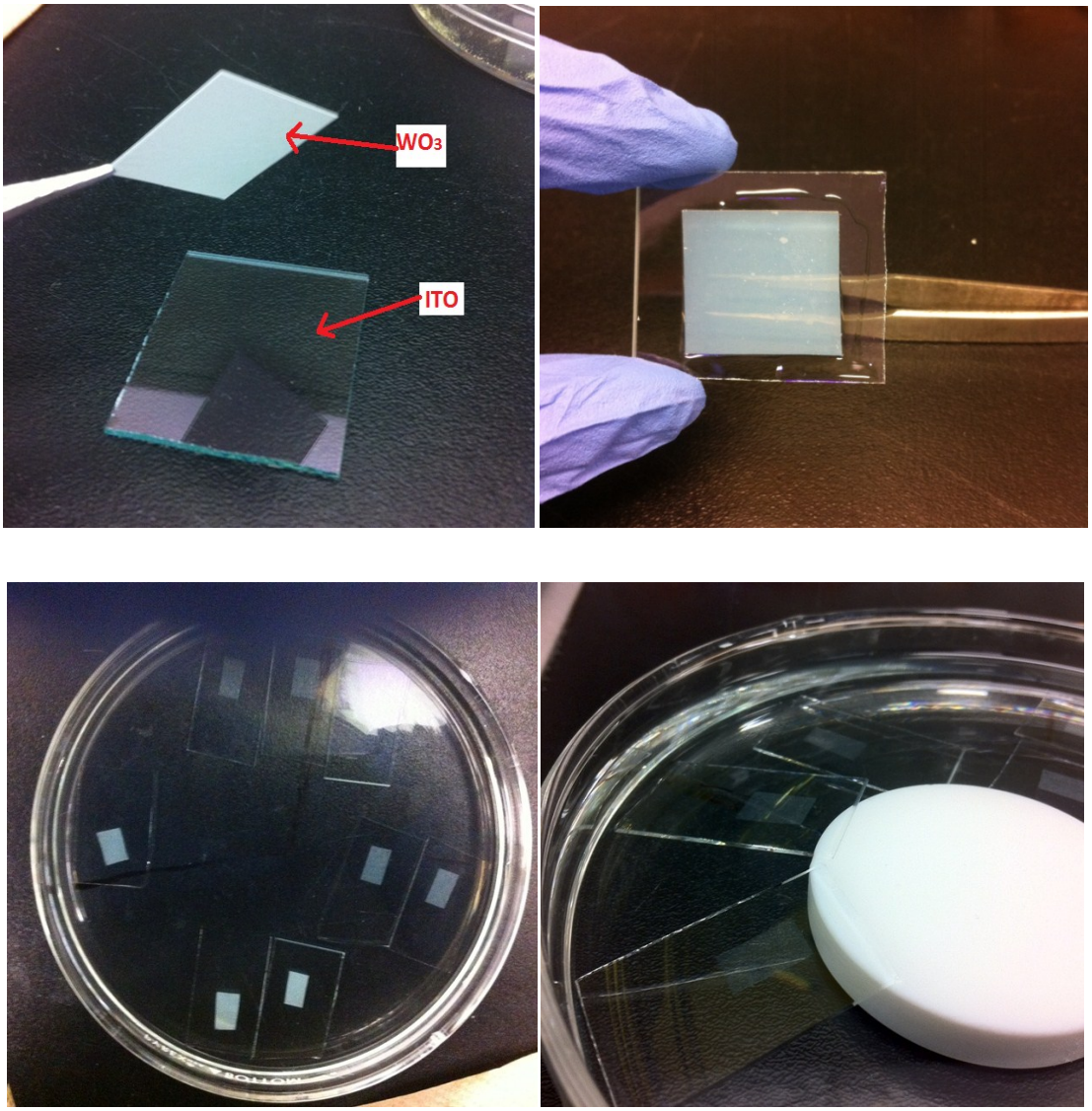

Figure 3.7: Deposition process. Filters with the particles side down were placed on the ITO face of substrate; top left, ODCB makes the interface adhesive; top right, samples in acetone bath to partially remove the filter (bottom left), samples tilted to completely remove the filter (bottom right).

In order to investigate the temperature dependence of morphology of tungsten oxide, some samples were subjected to a thermal treatment at specified temperatures for 1 hour.

3.5 Sample Identification

The samples were labeled based on the relative amount of tungsten oxide on the filters and the temperature at which samples were annealed. For an identical sample labeled "CT", the letter C represents the material on the filter which varies from 'I' to 'IV'. T represents the annealing temperature and is expressed in centigrade scale. 'R' is replaced with the temperature value if the sample is prepared at room temperature and was not annealed. Table 1 shows the films studied in this work.

Sample ID	IR	IIR	IIIR	IVR	I250	I500
Tungsten Oxide (mg)	1.25	2.5	5	10	1.25	1.25
Temperature (C)	25	25	25	25	250	500

Table 3.1: Sample identification: The value in the row of tungsten oxide is the amount of material used to prepare the filter.

3.6 Electrochemical Cell

Figure 3.8 illustrates the setup used for the electrochemical characterization of the samples. The electrochemical cell is a 5cm diameter and 9 cm height cylinder. The tungsten oxide film is considered as the working electrode, platinum the counter electrode and a 0.1 M sulphuric acid solution is the ion conducting electrolyte. In order to form the conventional three-electrode setup for the electrochemical measurements, the

working electrode which deposited on the ITO substrate is in contact with acid. The other side of the substrate is fastened on the electrochemical cell with two screws. Silver/silver chloride (Ag/AgCl) is immersed into the electrolyte as the reference electrode. It consist of a Teflon cap with a AgCl coated Ag wire sealed with a porous Teflon tip. Both counter and reference electrodes are from CH Instruments Inc.

The potential is applied between the working and reference electrode and the response such as charge transfer or current is measured between the working and counter electrodes.

Since the counter electrode is a non electrochromic material and is not positioned in the way of the incoming beam, the second transparent conductor is substituted with a glass slide which is a non-conductive (but transparent) material.

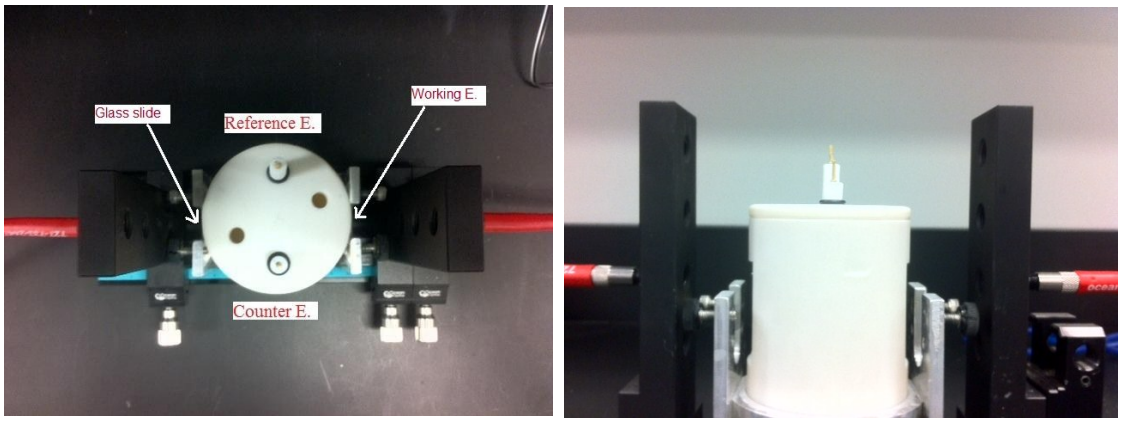

Top view Cross-section view

Figure 3.8: Device Setup

4. Characterization and Methodology

In order to investigate the electrochromic properties of an electrochromic material, electrochemical and optical techniques have been utilized. The methods include cyclic/linear sweeping voltammetry, chronoamperometry, chronocoulometry, electrochemical impedance spectroscopy and UV-VIS-IR transmittance, reflectance, and absorption. The following is a brief description of the methods used for measuring the characteristics of samples.

4.1 Physical Characterization

Scanning Electron Microscopy

The morphology of the samples was studied with a Hitachi S-4700 Scanning Electron Microscope (SEM) to investigate the microstructure and nanostructure of tungsten oxide films. In general, SEM emits a beam of electrons toward the sample and scans the backscatter electrons. SEM images are produced by the detected electrons emitted from the sample. The number of electrons that reach the detector depends on the topology and atomic weight of the films and their distance from the surface. Variation in these parameters gives rise to variation of the relative contrast of the SEM images. Thus good surface conductivity is a critical issue regarding SEM images. For nonconductive solid films, a layer of a conductive material is coated on them. In particular, coating prevents the accumulation of the static electric fields at the surface, improving contrast of the images.

As-deposited tungsten oxide films are generally semiconducting and a coating is indeed necessary. A thin layer of gold (of about 2.5 nm) was coated on the surface of the samples for 15 seconds by the sputtering process.

4.2 Electrochemical Characterization

The electrochemistry of the surface highly depends on the species, solution and electrodes immersed in the solution. An electrode reaction involves electron transfer between the two electrodes dipped in a solution where electron transfer results in the transformation of a material between the reduced and oxidation forms. In the case of an electrochromic material, the electrochemical reaction at the working electrode gives rise to a change in color or transparency. In order to measure the electrochemical properties of tungsten oxide films, electron transfer was carried out by two techniques. First, in cyclic voltammetry the applied voltage varies linearly between two optimum states going back and forth. In one state, the films were reduced and turned into a blue color, and in the other state, the films were oxidized to their original transparent mode. The current passing through the sample between the electrochromic material (working electrode) and the counter electrode is then measured and plotted versus voltage. In chronoamperometry, on the other hand, the potential, instead of having a linear time dependency, is stepped up between two voltages for a period of time and then stepped back to its initial value. The current passing through the sample is measured and plotted versus time.

All electrochemical measurements were carried out using the CH Instruments Inc. 604D electrochemical analyzer-workstation.

4.2.1 Cyclic Voltammetry

Application of a potential to an electrode and monitoring the corresponding current flowing through the electrode is the common characteristic of all voltammetric techniques used in determination of a variety of dissolved inorganic and organic substances [52]. Depending on the applied potential pulse method, one can refer to cyclic voltammetry (CV), normal pulse voltammetry (NPV), differential pulse voltammetry (DPV) and square-wave voltammetry (SWV) as examples of voltammetry. Particularly, in cycling voltammetry, the potential is linearly scanned from an initial voltage toward a higher (lower) voltage value in positive (negative) polarization with a certain speed (scan rate) and it scans back to the initial value. Figure 4.1 shows the diagram of the potential waveform applied as the function of time. The current is recorded as a function of the potential. CV patterns (also called voltammograms) give electrochemical information about the material under investigation [53] such as determination of kinetic parameters and mechanism. CV has also the ability to estimate the values of unknown parameters [52].

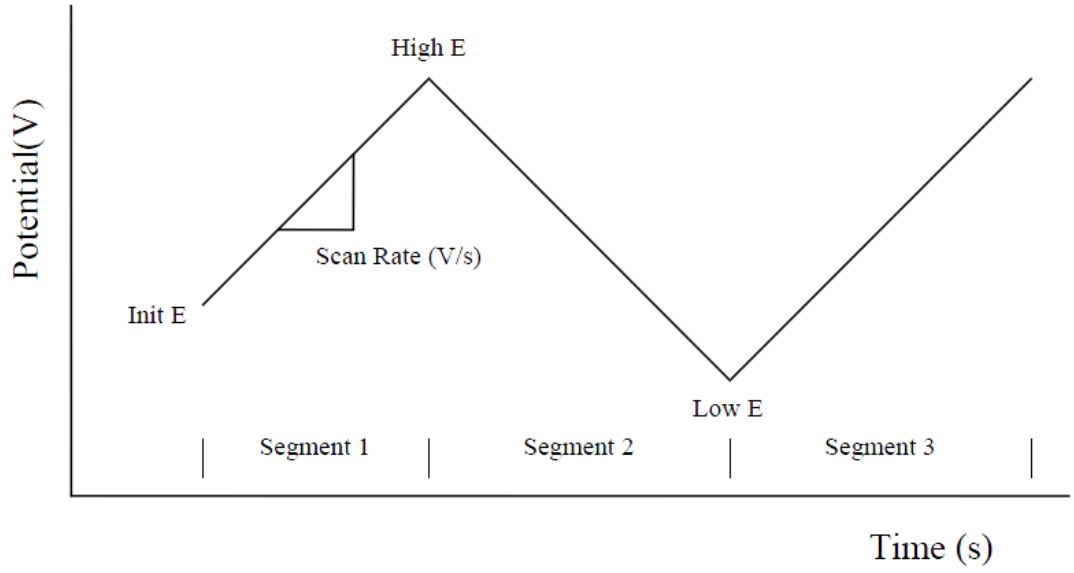

Figure 4.1: Diagram of the potential waveform vs. time during the CV (adapted from [54])

Cyclic voltammetry consists of two segments which are controlled by mass transport, electron transport and a mixture of the two [53]. The former can originate from ion migration, diffusion or both which is taking place inside the films. Migration is the movement of an ion in the presence of an electric field due to a potential gradient while diffusion is due to a concentration gradient. The electron, on the other hand, transports negative charges to the surface (reduction reaction). The rate of the reaction can be described by Butler-Volmer equation. Flux of electrons increases with time until the surface concentration becomes neutral. It thereafter starts to decrease (cathodic peak). At this point the process becomes diffusive. Likewise for oxidation process, an oxidation (anodic) peak will also appear if the redox couple is reversible.

For a reversible electrochemical reaction ($Ox + ne^- \Leftrightarrow Red$, in which Ox and Red are the oxidized and reduced form of the analyte, respectively) the application of a potential forces electrons to inject (extract) into (from) the analyte during the reduction (oxidation) process. The values of charges are not necessarily equal. The charge reversibility can be therefore identified as follows

$$\text{Charge reversibility} = Q_a/Q_{ca} \tag{4.1}$$

where Q_{ca} is the cathodic charge inserted during reduction and Q_a is the anodic charge extracted during oxidation.

4.2.2 Chronoamperometry

In Chronoamperometry (CA), the potential is stepped from an initial E value toward higher (lower) values in a positive (negative) polarity. In most cases CA is either carried out by a single potential step, in which only the current resulting from the forward step is recorded, or by a double potential step, in which the forward potential is returned to its final (initial) value following a time period (pulse width) . Figure 4.2 shows the diagram of the potential waveform applied as a function of time in a double potential step technique. The current can be recorded as a function of time. Likewise for CA, the applied potential is carried out between the working and reference electrodes and the responsive current passing through the working electrode is measured between the working and counter electrodes.

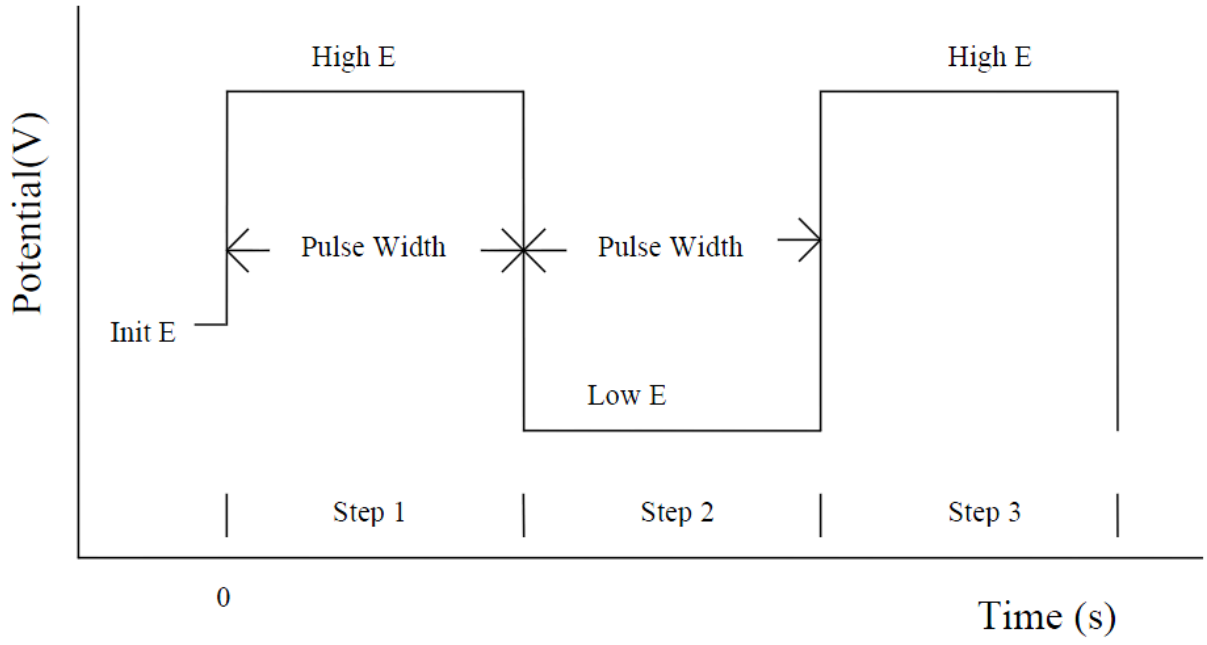

Figure 4.2: Diagram of the potential waveform vs. time in CA (adapted from [54])

We can consider that at the beginning of the experiment the analyte is all in the Ox. To ensure this assumption one can run a preconditioning setup before the experiment is started. When the potential is stepped up, Ox is converted to Red. The concentration of Ox is then decreased from its initial value until it becomes zero. Due to the occurrence of such a concentration gradient for Ox species, these latter diffuse toward the electrode surface until all Ox species reduce to Red and the current becomes zero. The current decay depends on the electroactive species and the kinetics of the reaction.

The most widely used equation in CA is the Cottrell equation which describes the measured current flowing through the electrode in a reversible reduction reaction, as follows

$$i_t = n\,F\,A\,C\,D^{1/2}/\pi^{1/2}\,t^{1/2} \qquad (4.2)$$

where n = stoichiometric number of electrons involved in the reaction; F is Faraday constant, A is the electrode area, C the concentration of the electroactive species and D is the diffusion coefficient of the electroactive species.

Following the same mechanism, for the reversible reactions, the backward potential step enforces the Red to oxidize to the original form of Ox. Moreover, the amount of charge transferred during the reduction and oxidization can be calculated from the CA curve by integrating of current versus time (I-t) patterns and the definition of charge reversibility would be also applicable here.

4.3 Optical Characterization

The insertion/extraction of ions and charge-balancing electrons results in a change in the optical appearance of the electrochromic films. These optical properties along with electrochemical properties can help to quantitatively describe the ionic transfer and how efficiently the ions induce the color change. To achieve this goal, a tungsten halogen light source, Ocean Optics HL-2000, provides a light beam going through the electrochemical cell. A fiber optic spectrometer, Ocean Optics USB2000+ collects the light from the other side of the electrochemical cell via the optical fiber in order to monitor it as shown in Figure 4.3. The obtained transmittance would be then

$$\%T_{\lambda} = I_0/I_i \times \%100 \tag{4.3}$$

where I_0 and I_i are the intensity of collected and incoming of light at wavelength λ respectively.

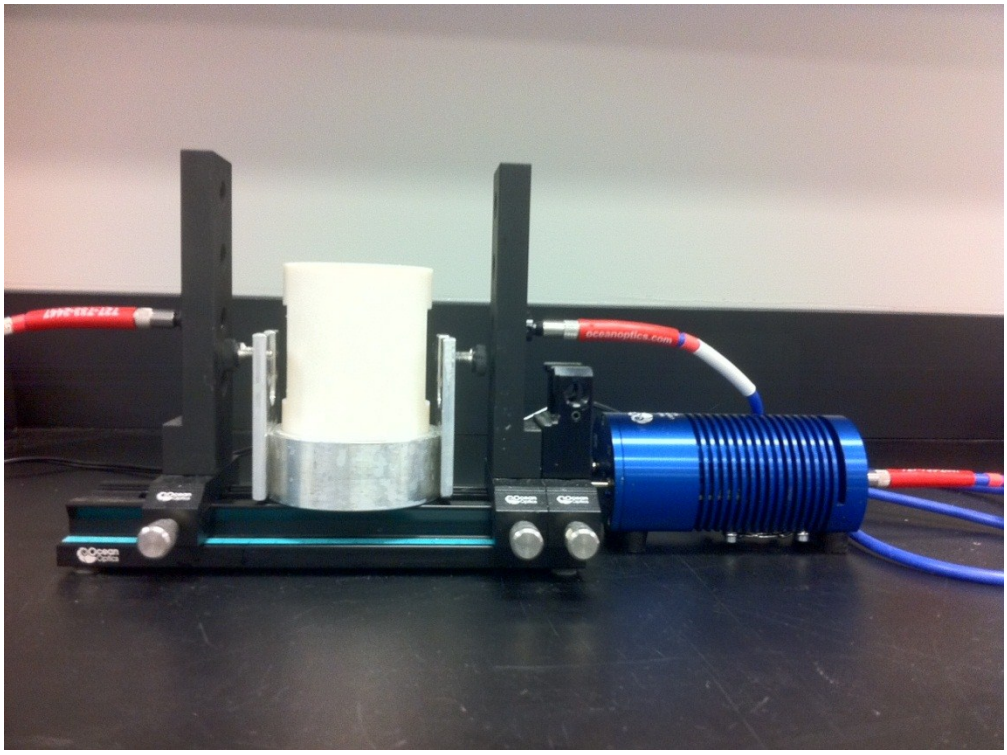

Figure 4.3: Optical measurement setup

The transmittance, in this study, was measured in the range of about 400 to 950 nm. The measurement was made in two different modes:

- Transmittance versus wavelength, at a specific time: This helps to monitor the optical behaviour of the electrochromic device at the extreme coloring and bleaching states. The overall optical modulation of the device can be also traced using these patterns.
- Transmittance versus time, at (a) specific wavelength(s): This approach, on the other hand, can give the detailed information about the coloring and bleaching

processes and at the switching point. If ΔT_λ has a large value we can expect high optical modulation at wavelength λ.

Reporting the optical properties of electrochromic devices, it is sometimes convenient to describe the optical modulations by optical density as follow

$$OD_\lambda = - \text{Log } T_\lambda \tag{4.4}$$

The optical density is also called optical absorbance (A_λ).

4.4 Other Key Parameters in Electrochromism

Optical reversibility

At wavelength λ, the optical reversibility is defined as

$$T_{\lambda,bl} \text{ after the coloring}/\ T_{\lambda,bl} \text{ before the coloring} \tag{4.5}$$

where $T_{\lambda,bl}$ is the transmittance of the electrochromic material at wavelength λ when it is in the bleached state.

Coloration Efficiency

The Coloration Efficiency (CE) is defined as the ratio of the absorbance change to the charge inserted (extracted) per unit electrode area.

$$CE_\lambda = \Delta OD_\lambda / Q \tag{4.6}$$

where Q is the charge density inserted (extracted).

Response time: The time needed for the electrochromic material to reach some fraction (normally above %90) of its maximum color or bleached state [11].

Life time

The well known definition of lifetime for an electrochromic device is the number of coloring-bleaching cycles that an electrochromic material can perform before any significant (electrochemical) degradation [11].

5. Results and Discussion

This chapter will present and discuss the results obtained from the different samples studied. The films used here for further investigation were taken from the samples identified in chapter 3. Although a large number of samples have been investigated, only a limited sampling is shown. The properties analyzed are typical of the films prepared in similar conditions of nanoparticles and thermal treatment.

5.1 Morphology and Structural Property

Figure 5.1 shows the SEM images of the nanoparticles films prepared at room temperature with the filtration and transfer technique. Films are generally a mixture of sparse particles and exhibit a far from continuous structure [55]. At room temperature, the morphology observed is composed of aggregates of various sizes of tungsten oxide nanoparticles. They indicate an average size of the smallest particles of about 50 nm which is consistent with the manufacturer's specifications. However, some particles are attached to their neighbours in different packing factors forming nanostructures larger than both the initial particles dispersed in the solution (less than 100 nm) and the pore size of the filters (namely 50 nm). These values are varying from 100 to 200 nm in the samples prepared with lower amounts of nanoparticles and up to 300 nm for the highest. Figure 5.1 also shows that the surface coverage increases gradually with the agglomeration of particles resulting in less porous films and smaller pore sizes. The

mesoporous structure of the walls separates the macropores in the tungsten oxide films [56].

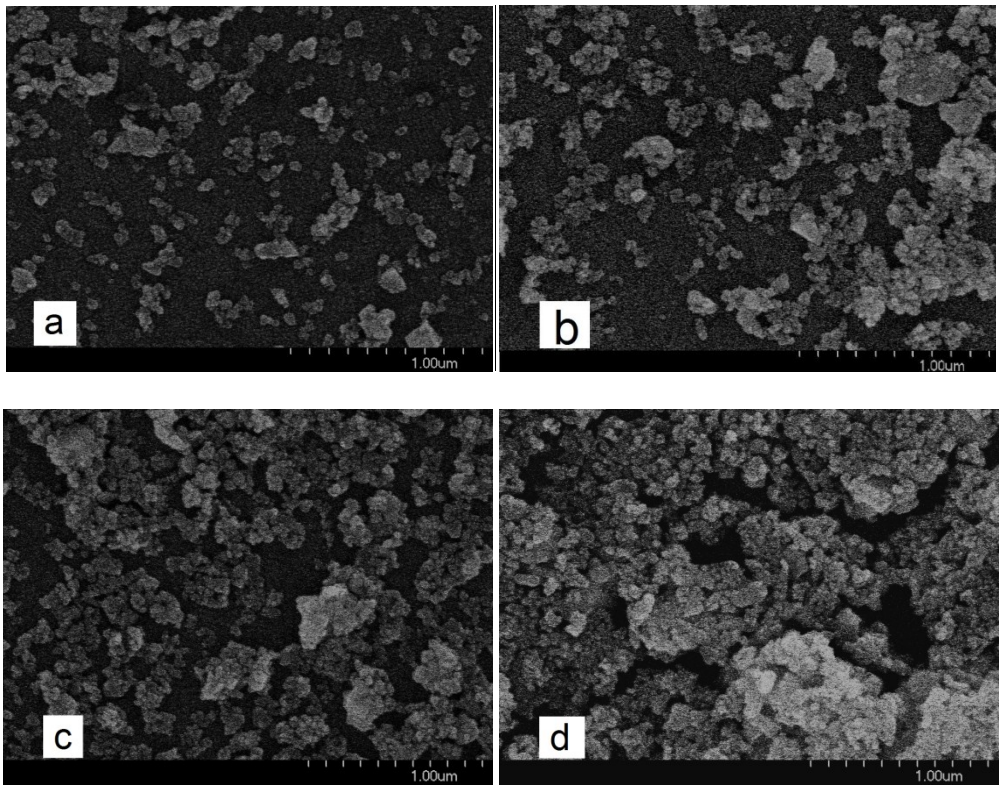

Figure 5.1: Surface view of SEM micrographs of tungsten oxide nanoparticles films deposited on ITO-glass at room temperature with the filtration technique: IR in 'a', IIR in 'b', IIIR in 'c' and IVR in 'd'

As for other recent fabrication techniques, the thickness of the films prepared in this study was found to be depending on preparation conditions [12] [13], in this particular case on the amount of nanoparticles. The thickness was estimated from the SEM taken at cross-section of the films by using an inclined holder and tilting the sample, as shown in Figure 5.2. The thickness is represented by the average agglomerates height varied from 5 to more than 10 μm.

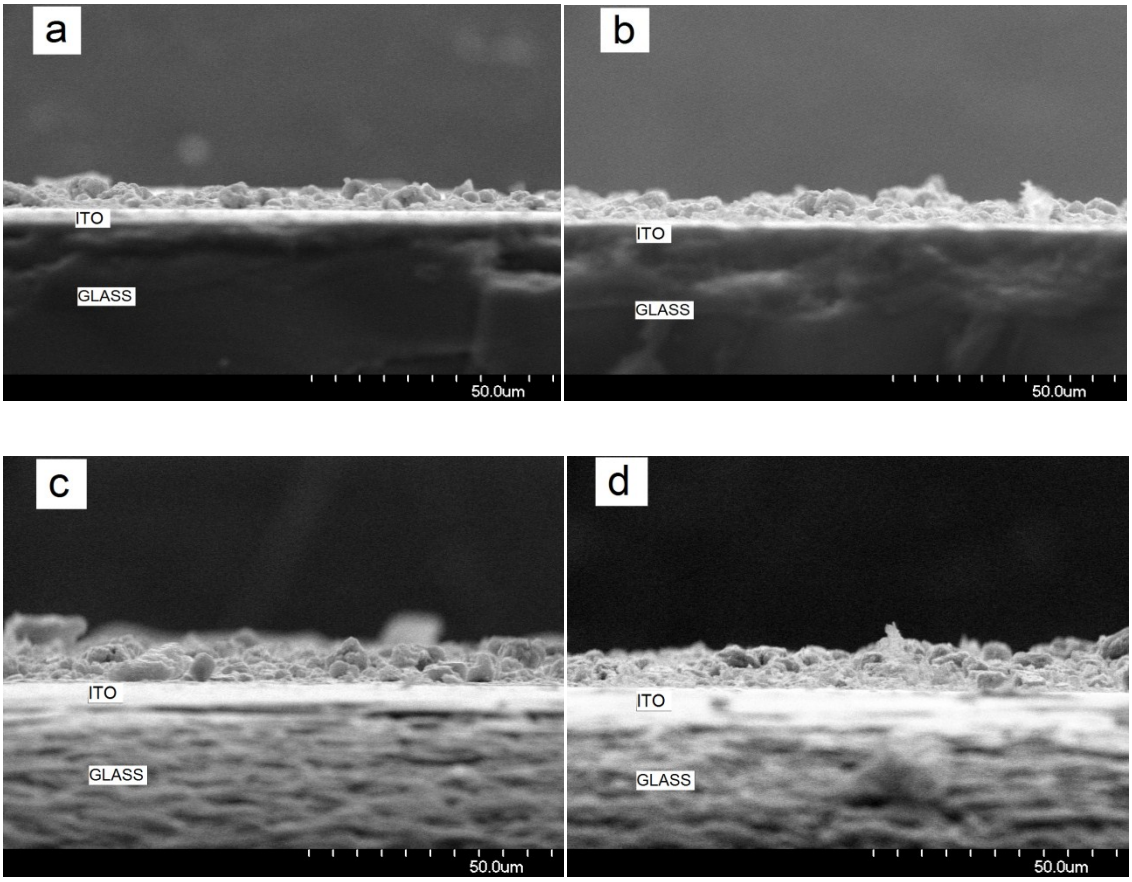

Figure 5.2: Cross-section view of SEM micrographs of tungsten oxide films deposited on ITO-glass with the filtration technique: IR in ‘a’, IIR in ‘b’, IIIR in ‘c’ and IVR in ‘d’

It clearly shows that an increase in the amount of nanoparticles results in thicker films. In comparison with the nanostructured films prepared with other techniques, these films are thicker [57] [58] [59]. Although the amount of nanoparticles in the suspensions was 1.25, 2.5,5 and 10 mg for the samples IR, IIR, IIIR and IVR respectively, the thickness of the films was not necessarily doubled. Instead, samples prepared with higher amounts demonstrate more massive and dense structures on the surface. This presentation of the films in dense samples results in high optical diffusion of light and can further affect their overall appearance. As shown in Figure 5.3, films that were prepared with higher amount of nanoparticles exhibit a prominent milky color appearance.

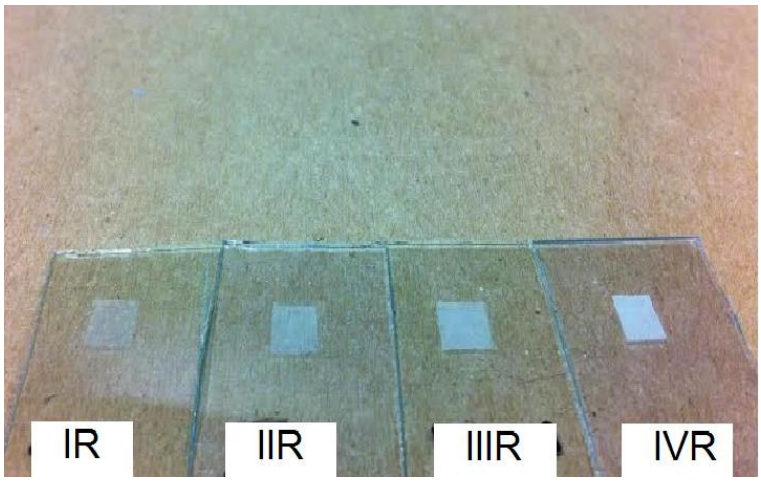

Figure 5.3: Optical appearances of as-deposited samples

In order to quantitatively compare the optical appearances of the samples we measured the transmittance of as-deposited samples as shown in Figure 5.4.

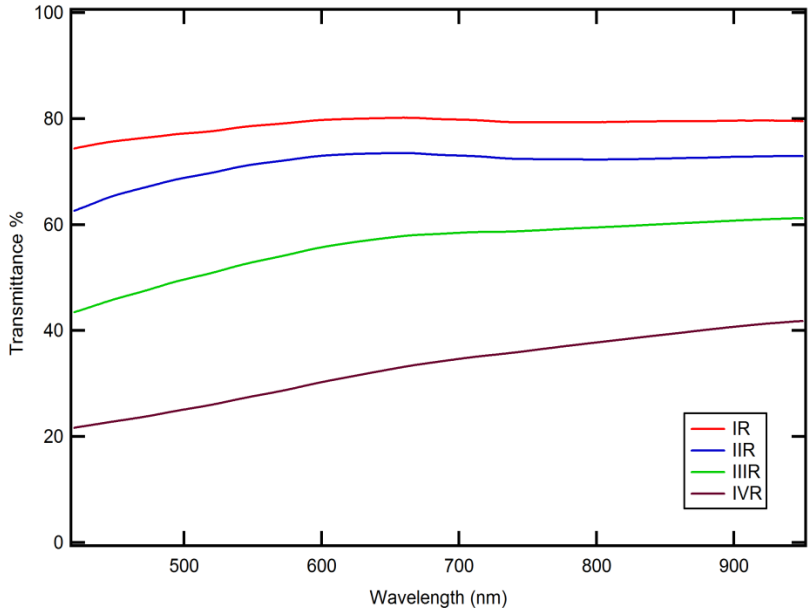

Figure 5.4: Transmittance spectrum of the as-deposited samples prepared with different amounts of tungsten oxide nanoparticles.

As expected, the transmittance spectrum clearly indicates that it has a reciprocal relationship with the thickness and density of the films. Dense films back-scatter the incoming light more than the thinner films, giving rise to lower transmittance.

In order to study the annealing effect on the structure of the films, some samples were subjected to thermal treatments at 250 and 500^{o}C. As shown in Figure 5.5, at these temperatures, particles were highly packed together.

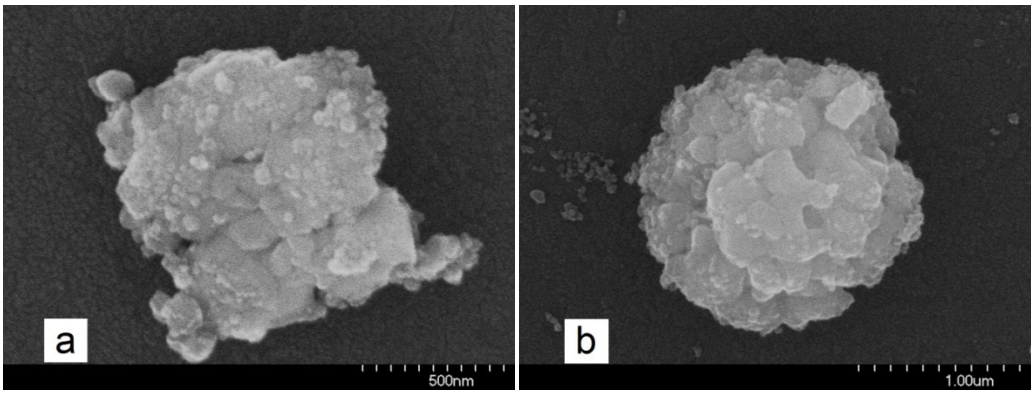

Figure 5.5: Surface view of SEM micrographs of tungsten oxide films deposited on ITO-glass with the filtration technique annealed at 250^{o}C, a, and 500^{o}C, b

Packing size in the annealed films was higher than that observed for concentrated films. Aggregation of the particles results in the formation of very large microstructures with an average size up to 3 and 10 μm (which are not shown here) for the samples annealed at 250 and 500^{o}C respectively. It has been observed by Cronin et al. [60] that a crystalline phase appears at 182^{o}C for the films prepared by spin and dip coating. It has been also reported that further increase in annealing temperature results in improvement in the crystallinity of the films [61] [62] [16]. Moreover, when particles of an area pack tightly

together it creates more room in the background of that area. It should be noted that there is still a fraction of particles that is left unpacked in the annealed samples as well as in the non-annealed ones.

It is worth looking in more detail at the packing process in the annealed samples. Figure 5.6 shows the structure of a sample annealed at 500^{o}C at different magnifications.

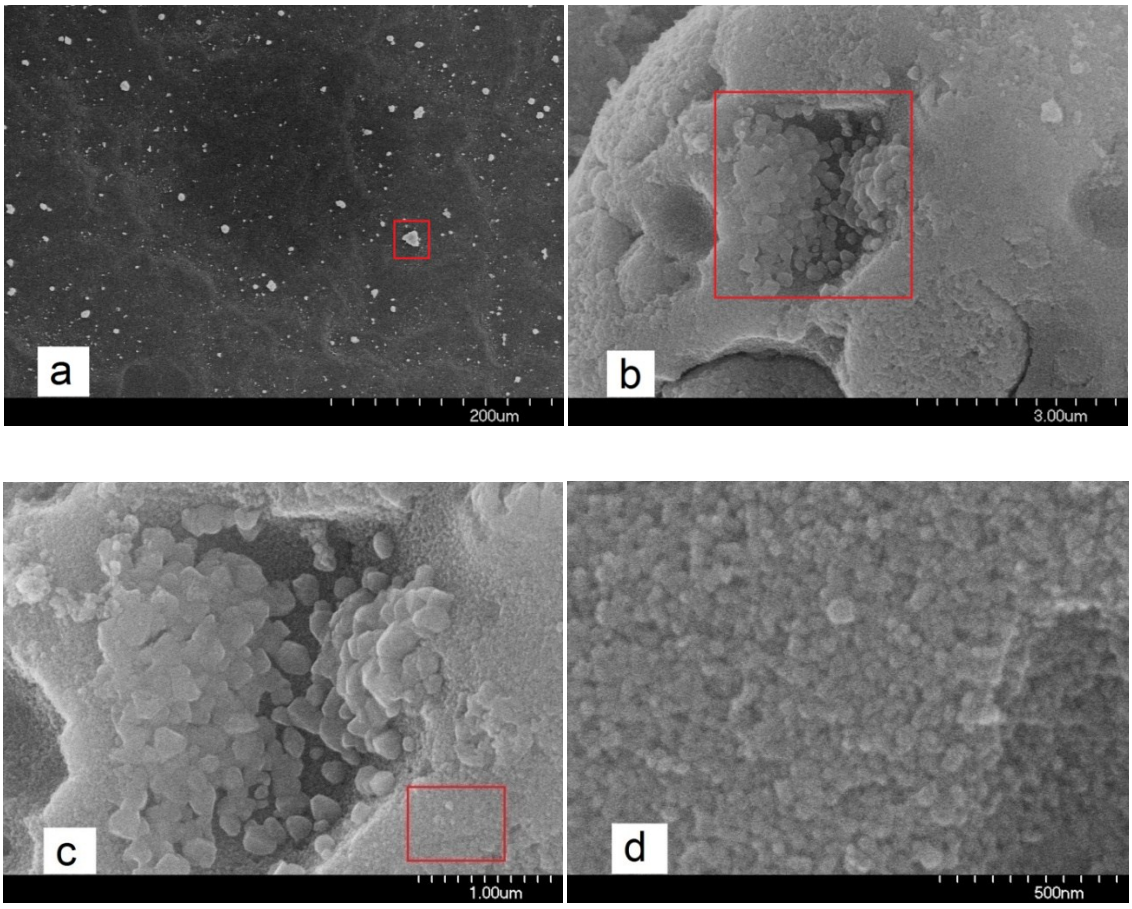

Figure 5.6: Packing process in a tungsten oxide film annealed at 500^{o}C (Sample I500). The red box in each image is magnified in the following image, starting from ‘a’and finishing in ‘d’.

In ‘a’, we can observe the irregularities on the surface of the sample in a large scale which are generally in form of local microstructures. One of these microstructures (red

box) is zoomed in different magnifications in ‘b’ and ‘c’. We can see that these microstructures are indeed comprised of relatively small tungsten oxide compounds that tend to aggregate toward the surface and form larger structures. However, aggregation in different spots of a microstructure takes places at different rates and in different fashions. Highest magnification in ‘d’ clearly indicates that at the heart of these large structures are nanostructures of tungsten oxide with an average size of 50 nm that are uniformly organized.

The contrast in the particle size at large scale originates in different irregularities on the surface of annealed samples that diffuse light more than the non-annealed ones. Figure 5.7 shows the optical transmittance of a sample treated at different annealing temperatures. It shows that the overall transmittance spectrum is slightly lower for samples whose preparations were followed by a thermal treatment.

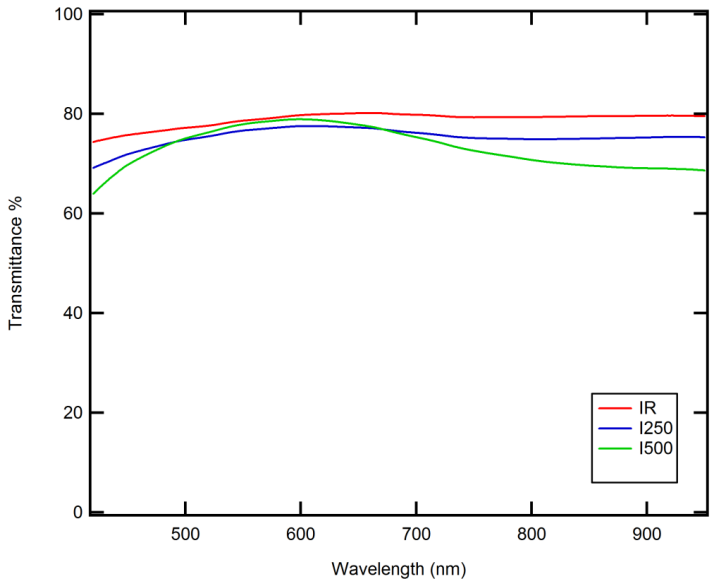

Figure 5.7: Transmittance spectrum of the as-deposited samples prepared at different annealing temperatures

More interestingly, it has been seen that the thermal treatment for very dense samples results in more uniform aggregation and similar packing at both micro- and nano- scale. Figure 5.8 shows sample IV before and after annealing. The packing process is the same as illustrated above but with a notable difference: in this case, particles tend to form a larger crystalline structure. Souza [63] attributed the formation of crystalline structures in WO_3 films annealed at 500^oC to the alteration of the W-O stretching modes in WO_6 octahedral units. The dimension of the most microstructures falls between 1 and 1.5 μm.

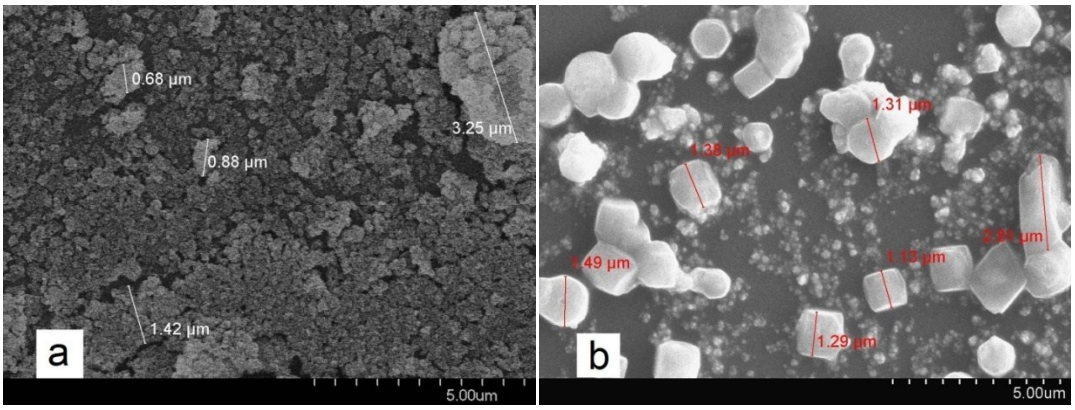

Figure 5.8: Surface views of SEM micrographs of sample IV at room temperature, a, and after thermal treatment, b

5.2 Electrochemical Techniques

5.2.1 Cyclic Voltammetry (CV)

Electrochemical Property

Some electrochromic materials need to be activated before any electrochemical experiments are conducted and validated. Activation is usually done by a linear potential

varying technique such as CV [64]. It activates all available vacant sites in the tungsten oxide film and equilibrates them. As shown in Figure 5.9, the activation is evaluated by the voltammograms obtaining from the potential range between -1 to 0.5 V versus Ag/AgCl reference electrode in a 0.1 M H_2SO_4. The anodic current increases with the number of cycles. The origin of so called cycling-driven activation is most likely due to the nature of the films that limits the proton diffusion, as neither the surface structure nor the thickness were modified after activation [65]. In our recent work, it has been seen that a 10 to 15 cycle preconditioning assures the stability of the sites. After activation, the voltammograms, as expected, reach a stable pattern and the hydrogen insertion/extraction rate reaches a constant value as the sites (involved in the diffusion) becomes saturated [66].

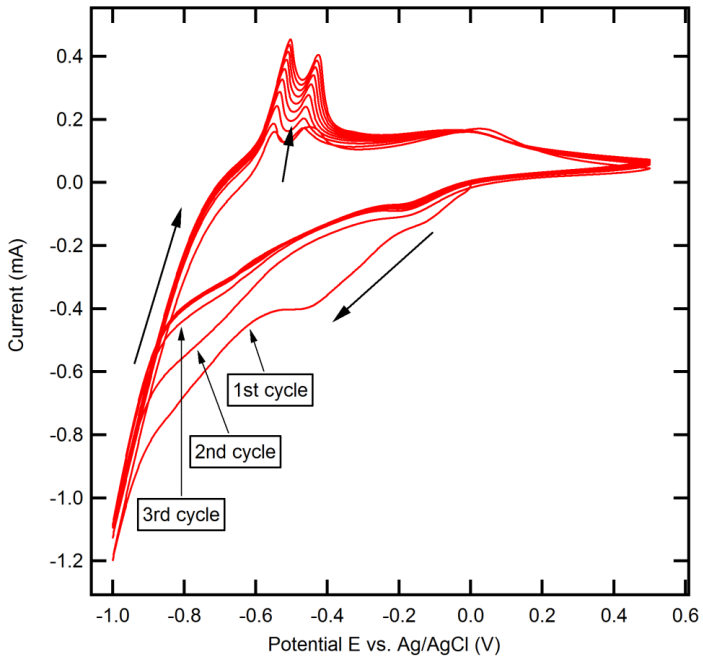

Figure 5.9: Activation process for sample IV500. Offset arrows represent scanning direction and inset arrows represent the evolution of voltammograms as the number of cycles increases during the activation.

The activation process is shown in Figure 5.10 ‘a’ and ‘b’ for the samples prepared with different amounts of nanoparticles and at different annealing temperatures, respectively.

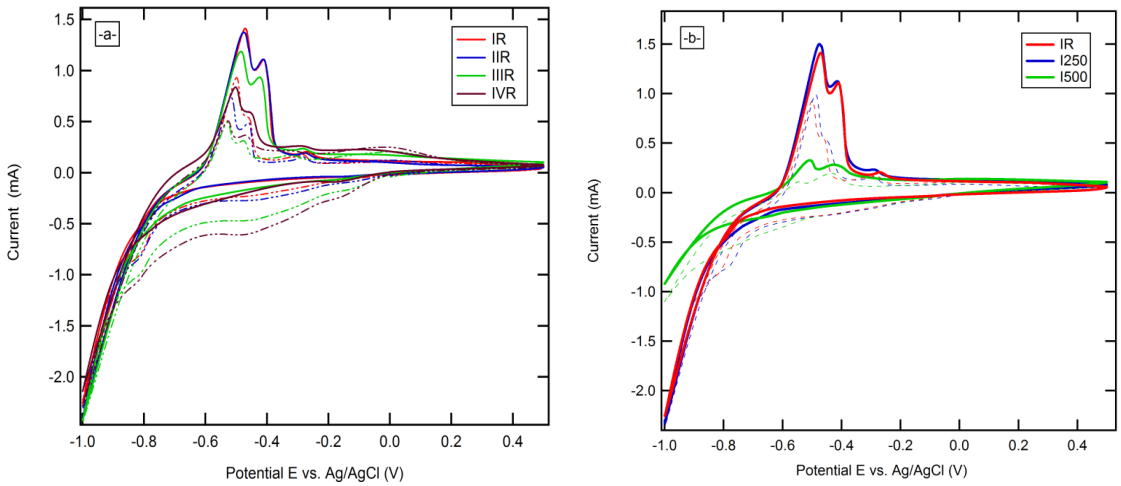

Figure 5.10: Voltammogram before (dashed) and after (solid line of the same color) activation for samples prepared with different thicknesses, a, and different annealing temperatures, b. Scan rate was set equal to 0.05 V/s.

Multiple anodic (oxidation) current peaks are clearly defined for all samples. There are two high anodic current peaks taking place at anodic potential range between -0.6 and -0.4 V. For non-annealed samples, in Figure 5.10 ‘a’, there are also two small anodic peaks, which are lower and broader and taking place at potentials around -0.3 and 0 V. The development of such behaviour during ion extraction (deintercalation) has been reported previously [44] [66] [67] [68]. Kim and Pyun attributed these anodic peaks to three types of hydrogen sites in a sulphuric acid based electrolyte electrochromic device: (1) reversibly active site, (2) shallow reversibly trap site and (3) deep irreversibly trap site. Thinner films exhibit higher anodic peaks and therefore faster hydrogen kinetics.

Beside the mentioned peaks, for annealed samples as shown in Figure 5.10 'b', there is one small anodic peak that can be observed around -0.25 V. Samples annealed at 250^{o}C exhibit slightly higher anodic peaks than of those prepared at room temperature but have almost the same overall pattern. Annealing at higher temperatures decreases the number of trap sites in the film which results in lower peaks [69]. Samples annealed at 500^{o}C exhibit smaller patterns and lower peaks. The evolution of the voltammograms and anodic peaks during the activation is also smaller in these samples. Anodic peaks increase only to 0.2 mA as compared to 0.4 to 0.7 mA in non-annealed samples and those annealed at 250^{o}C.

Two cathodic (reduction) peaks at -0.1 and -0.5 V can also be observed for non-annealed samples. Peaks for thicker films are clearer in Figure 5.10 'a'. It has been reported that tungsten oxide could form stable tungsten bronze forms during the hydrogen insertion [45] and these peaks could refer to these bronzes. These peaks however disappear after the activation. Annealed samples show the same trend.

Although samples with different thicknesses and annealing temperatures indicate distinct peaks, all samples exhibit an increase in the anodic peaks during the activation which reveals the fact that the insertion coefficient x increases and the kinetics of proton becomes faster as cycling proceeds (end of activation).

Besides, the cycling stability of the films shows that the current decreases after the 350th cycle for annealed sample at 500^{o}C. This number is however lower for non-annealed and annealed samples at 250^{o}C. In general, samples that were annealed at temperatures above 400^{o}C (which are not all mentioned here) demonstrate better stability.

Electrochromic Performance

Figure 5.11 shows the optical modulation of sample IV500 ‘b’ for a CV experiment ‘a’ at scan rate of 0.1 V/s. During each scan, tungsten oxide films undergo reversible coloring and bleaching.

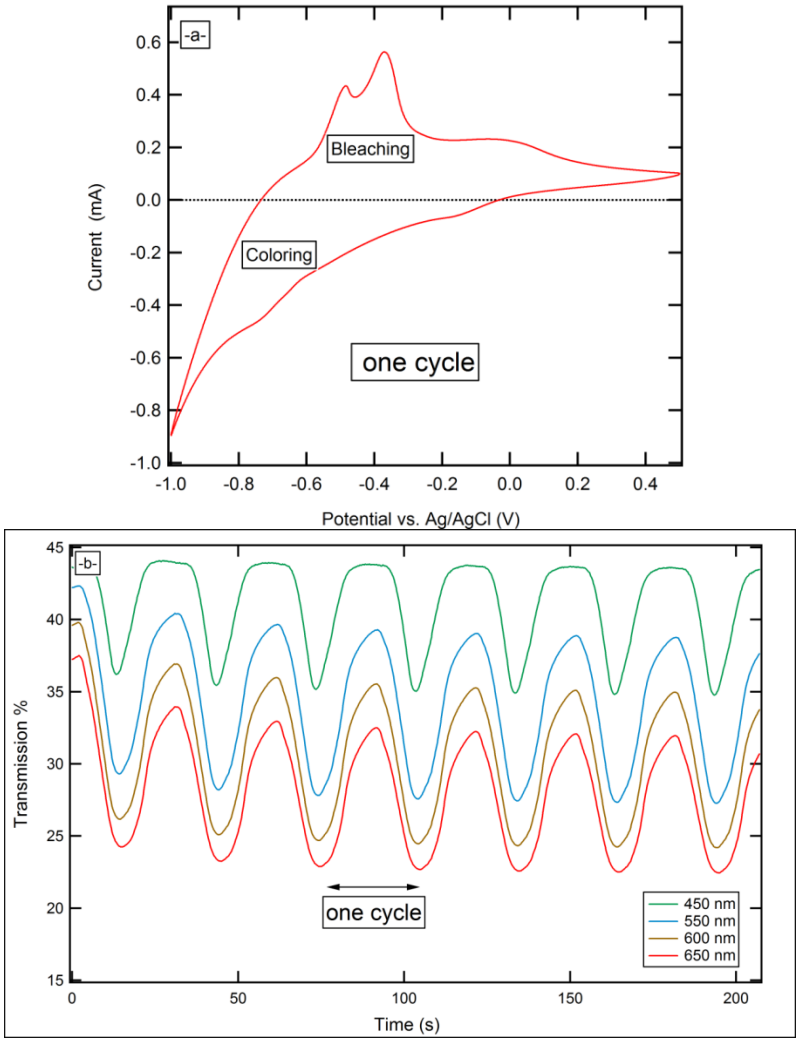

Figure 5.11 Electrochromism in terms of CV for sample IV500, a, and optical modulation response to it, b; scan rate was set to 0.1 V/s.

The optical density (OD) is plotted for the sample at wavelength 600 nm versus time along with the voltammogram as shown in Figure 5.12.

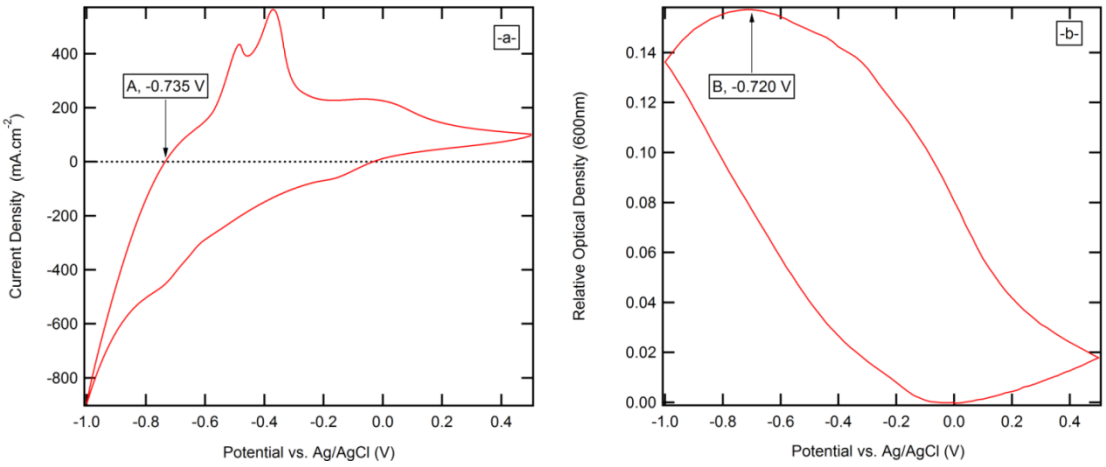

Figure 5.12: Voltammogram of sample IV500, a, and corresponding optical density, b

We can observe that the current density changes its sign at E= -0.735 V (point A in Figure 5.12a). At this point a maximum charge has been inserted into the host matrix. This is equivalent to saying that *x* in H_xWO_3 has reached its maximum value. Coloration, on the other hand, reaches its maximum at E= -0.720 V (point B, Figure 5.12b). Therefore, the maximum of the OD (-chromism) occurs 0.015 V, or 0.15 seconds (from the scan rate), after the maximum of current density (electro-). It other words, the kinetics of coloration is a little slower than the kinetics for electrochemical reaction. This lag in time is due to the diffusion behaviour of ions while being injected into the films. This phenomenon has been already seen in an acidic electrolyte [70]. Vuilleminet et al. reported a one to two seconds delay for such behaviour for hydrogen ions in tungsten oxide. Their reported chemical diffusion coefficient, however, was of the order of 10^{-10} - 10^{-11} cm^2s^{-1}. As a matter of fact, we should anticipate a higher value of the diffusion coefficient. Details of the diffusion behaviour of protons will be discussed later.

The charge density and the rate of coloration (dOD/dt) have been plotted as a function of the potential in Figure 5.13.

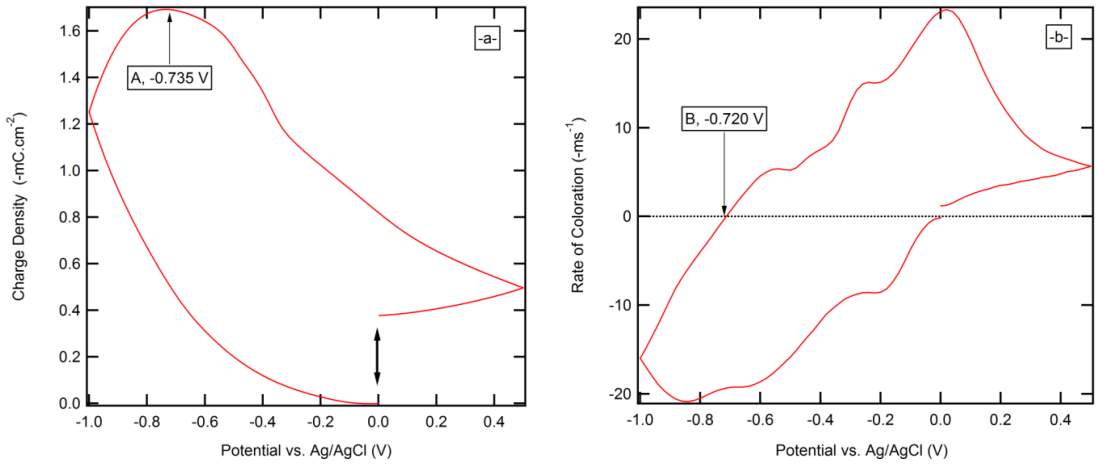

Figure 5.13: Charge density pattern during CV technique, a, and rate of coloration, b

The inserted charge density was obtained by the integration of the current density versus time (Figure 5.13 'a') and the rate of coloration from differentiation of OD versus time (Figure 5.13 'b'). As coloring takes place in the tungsten oxide film, a large amount of charge is inserted into the film but not all is extracted when the film is bleached (open-ended appearance in Figure 5.13 'a'). The reason for such behaviour is the existence of the trap sites. Moreover, we used a diluted electrolyte (0.1M sulphuric acid), therefore there is a large amount of molecules of water in contact with the films at the interface of the film and the electrolyte. This could result in the formation of $W(OH)_x$ [71].

Like for Figure 5.12, point A on the Figure 5.13 'a' shows the maximum inserted charge into the WO_3 film that occurs at E= -0.734 V. Coloration reaction, on the other hand, reaches its maximum at point B in Figure 5.13 'b' which is at E= -0.720 V. It has been accepted that charge reversibility enforces optical reversibility [13]. We have, however,

shown that the other way is not necessarily wrong: weak charge reversibility *may* result in high optical reversibility.

At low scan rates the electrochemical reactions at the surface of the electrodes take place in almost a steady state manner. The lower the scan rate, the more time is required for each cycle and the higher is the optical modulation. Figure 5.14 shows the optical density (absorbance) of the extreme states during the CV experiment with a scan rate of 0.005 V/s. Compared to the values shown in 5.11 ‘b’ that exhibits lower ODs (less than 0.2) it reveals the importance of choosing the appropriate scan rate in the optical properties of an electrochromic device.

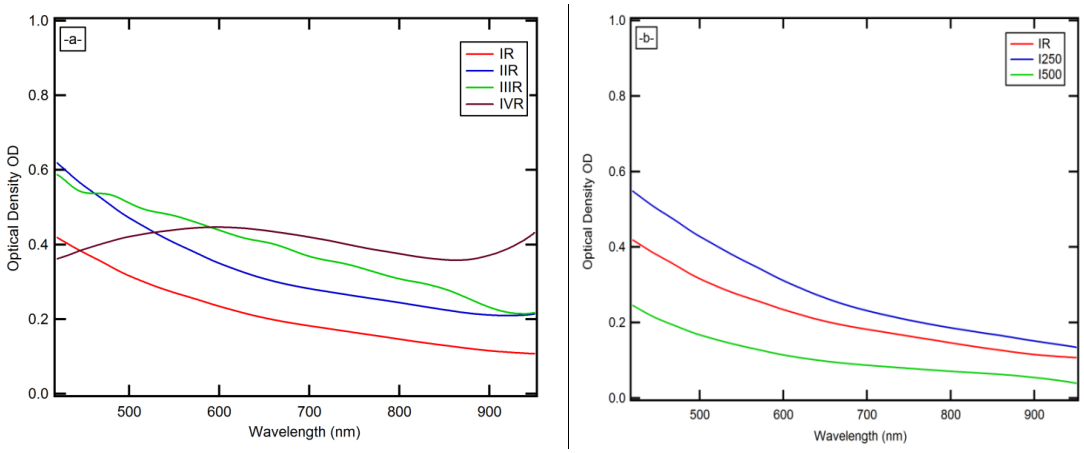

Figure 5.14: In-situ optical density of the samples prepared with different amounts of nanoparticles, a, and at different annealing temperatures, b. Optical densities of bleached states were set equal to zero. Scan rate was set to 0.005 V/s.

5.2.2 Chronoamperometry (CA)

Electrochemical Property

Figure 5.15 ‘a’ represents a chronoamperometric plot obtained by applying a step functional potential of 30 seconds for coloring and bleaching, corresponding to E_i and to +0.5 V, respectively; where E_i was set to -0.5, -0.6, -0.7, -0.8, -0.9 and -1 V. Each segment was preceded by a 30 second preconditioning at +0.5 V. The preconditioning removes the unwanted charge insertion during initial open-circuit condition and ensures that the measured charge values are verified. For all applied voltages, the current density peak for bleaching is higher than that of coloration and the current density during bleaching decays faster than coloration. This is a typical characteristic of tungsten oxide when inserted/extracted ions are small [72].The higher bleaching current arises from good conductivity of HWO_3 bronze and the rapid current decay is due to the conductor HWO_3 to the semiconductor WO_3 transition while the coloring kinetics is slower.

In Figure 5.15 ‘b’ the charge density exchange during the coloring- (proton insertion, cathodic charge, Q_{ca}) and the bleaching process (proton extraction, anodic charge, Q_a) were calculated by the integration of the curves in Figure 5.15 ‘a’ between starting and ending times of each segment as follows:

$$Q = \int J_{(t)} dt \tag{5.1}$$

Charge reversibility can be therefore obtained by Q_a/Q_{ca} [66]. The fact that the inserted and extracted charges are similar indicates a high reversibility of the electrochromic coloration/bleaching process and is considered as a desirable characteristic of electrochromic devices [12]. Calculated Q_a, Q_{ca} and charge reversibility for different applied potentials and different samples are reported later in table 5.1 in order to discuss the electrochromic performance. It should be noted that the mature technique for the

study of charge transfer in electrochromic material is chronocoulometry (CC), in which, charge exchange ratios are obtained directly by the electrochemical analyzer during reduction/oxidation reaction. Due to the high correlation of results for CA and CC, we only report the CA results here.

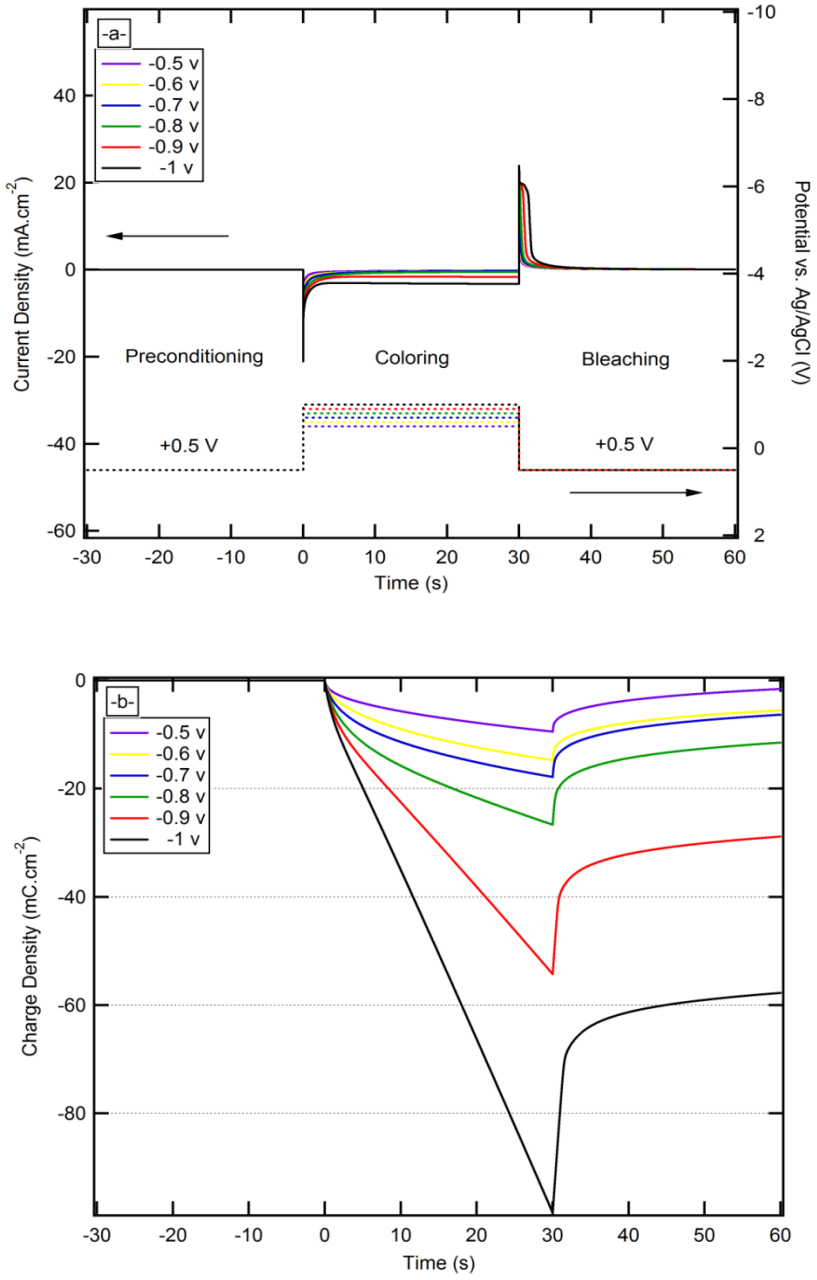

Figure 5.15: Current density, a, and charge density, b, of sample IV500 in CA experiment

Electrochromic Performance

The coloring and bleaching processes were measured under the application of negatively (cathodic) and positively (anodic) polarized voltage, respectively that were associated with the proton insertion and extraction. For the sample used in the CA measurement above, the in situ transmittance spectra were obtained simultaneously by the spectrometer during the coloration as shown in Figure 5.16. From this figure, one can see the variation of transmittance spectra in the visible range of the film between different colored states. These states are associated with the number of color centers depending on the number of inserted protons and electrons into the electrode. The transmittance at λ = 550 nm (the sensitivity peak of human eye [12]) decreases from 48% to 27% corresponding respectively to a potential of +0.5 V and -1 V.

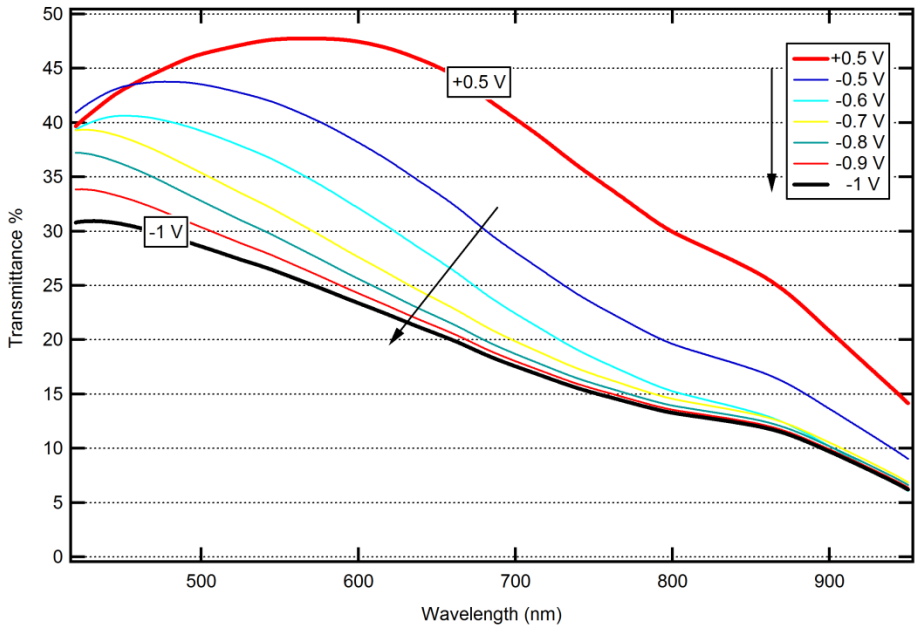

Figure 5.16: Transmittance of sample IV500 (ct. Figure 5.15) at different cathodic potentials

These patterns are unique for each sample. As an example, Figure 5.16 shows that the main part of coloration takes places during the application of cathodic potential at -0.7 V and -0.8 V and color of the film slightly changes at -0.9 V to -1 V. This is not necessarily true for non-annealed samples where a large portion of coloration takes place at -0.9 V and -1 V (Figure 5.17).

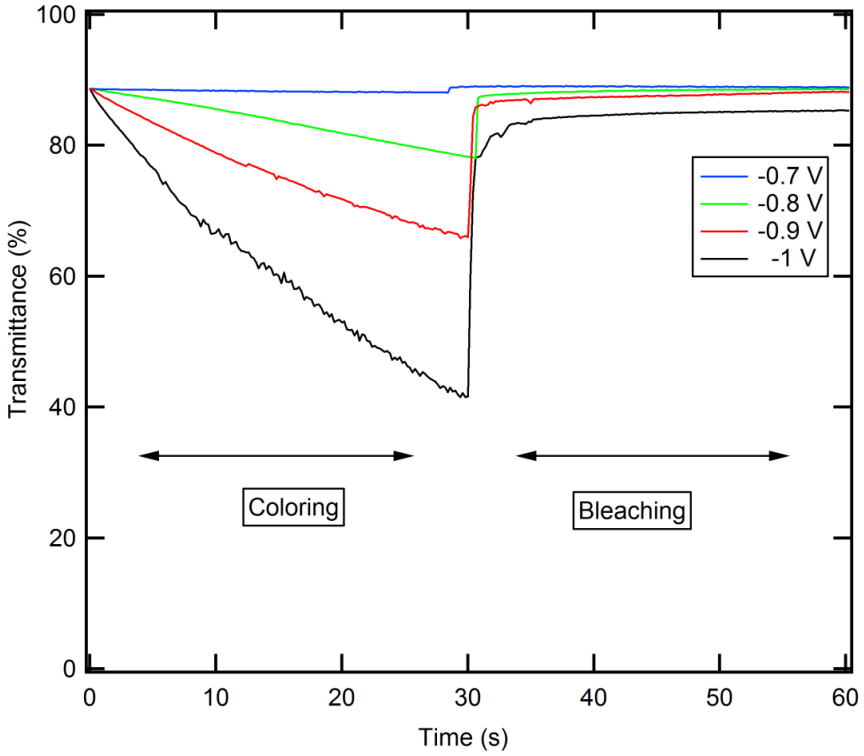

Figure 5.17: Time-dependent transmittance of sample IR during electrochromic performance for wavelength 450 nm

Other samples which prepared with different amounts of nanoparticles and at different annealing temperatures have been also measured with a similar CA technique and the final results are summarized in Table 5.1. As expected, higher applied potential implies higher insertion of charges and higher optical densities. In comparison with the results reported previously for single and mixed electrochromic WO_3 [56] [12], the optical

modulation at the visible range for WO_3/ITO at shorter wavelengths is improved in this study. Herein, sample IIR attains a ΔT at λ = 450 nm (ΔT_{450}) more than 51% upon coloring and bleaching. This wavelength is correspondent to the blue color.

Sample ID	Electrochemical properties				ΔT (%)		Opt. Rev. (%)	
	E_i (v)	Q_{ca} (mC)	Q_a (mC)	Q_a/Q_{ca}(%)	450nm	650nm	450nm	650nm
IR	-0.6	3.79	2.26	60	<1	2.30	>99.9	100
	-0.7	5.12	2.41	47	3.90	4.20	100	99.7
	-0.8	10.7	4.15	39	10.6	4.80	99.8	99.3
	0.9	37.8	14.4	38	22.7	11.3	99.4	99.1
	-1.0	73.0	27.1	37	46.9	30.6	96.4	93.6
IIR	-0.6	3.51	3.30	94	2.10	4.70	100	100
	-0.7	5.17	3.22	62	4.20	5.20	100	99.2
	-0.8	9.77	4.99	51	10.0	8.10	100	96.7
	0.9	23.1	11.6	50	35.4	17.9	100	95.4
	-1.0	32.0	16.0	50	51.2	35.7	94.3	93.2
IIIR	-0.6	4.31	3.55	82	3.80	11.0	100	100
	-0.7	6.45	3.74	58	4.60	15.7	100	94.6
	-0.8	11.3	5.53	49	11.6	18.7	100	90.4
	0.9	38.7	15.8	41	25.6	23.2	100	93.0
	-1.0	79.4	30.5	38	35.6	31.7	100	92.2
IVR	-0.6	3.68	3.01	82	3.50	4.10	100	98.3
	-0.7	5.48	3.32	61	4.20	7.20	100	91.4
	-0.8	11.1	5.21	47	8.60	15.1	100	84.3
	0.9	41.4	15.5	37	17.4	17.5	100	85.6
	-1.0	83.9	30.2	36	22.3	19.3	100	89.2
I250	-0.6	3.59	2.23	62	2.00	8.10	100	98.5
	-0.7	4.61	2.37	51	3.30	9.70	100	96.9
	-0.8	8.77	4.87	56	12.6	11.7	100	97.5
	0.9	33.3	20.5	62	31.4	22.3	99.8	98.2
	-1.0	67.7	42.1	62	38.4	30.2	100	98.3
I500	-0.6	3.79	2.19	58	N/A	5.10	N/A	100
	-0.7	4.15	2.70	65	N/A	5.60	N/A	100
	-0.8	6.22	3.73	60	N/A	9.00	N/A	97.5
	0.9	16.2	8.99	56	N/A	11.7	N/A	98.1
	-1.0	30.9	16.9	55	N/A	20.0	N/A	98.2

Table 5.1: Electrochromic results from CA technique for the samples with different preparation characterizations (first column), applied potential stepped from +0.5 V to the values of E_i (second column) and stepped back to +0.5 V, third and fourth columns are charge inserted and extracted charges, Q_{ca} and Q_a, respectively; charge reversibility is shown by Q_{ca}/Q_a. Last four columns are optical modulation and optical reversibility at wavelengths 450 and 650 nm.

For longer wavelengths ($T_{700-800}$), on the other hand, the optical modulation was smaller. This would result from the H_2SO_4/WO_3/ITO absorption at longer wavelengths. Like for CV measurements, a fraction of the charge remains in the tungsten oxide trap sites and the rest is driven out during the bleaching process. Table 5.1 also indicates that optical reversibility has higher values for the samples that underwent cycling through lower potentials and, that basically, higher insertion results in lower charge stability. From these results we can conclude that:

1) Higher applied potential results in higher charge insertion/extraction, an increase in optical modulation and decrease in charge and optical reversibility, and vice versa.
2) Optical reversibility has always higher values than charge reversibility disregarding applied potential. We can state that the amount of inserted charges that stay in the trap sites during the bleaching are not involved in the coloration process.
3) Open-ended pattern for charge density and close-ended pattern for OD in CV technique are consistent with the results obtained from CA.

Figure 5.18 shows the appearance of samples when are under coloring/bleaching with CA technique.

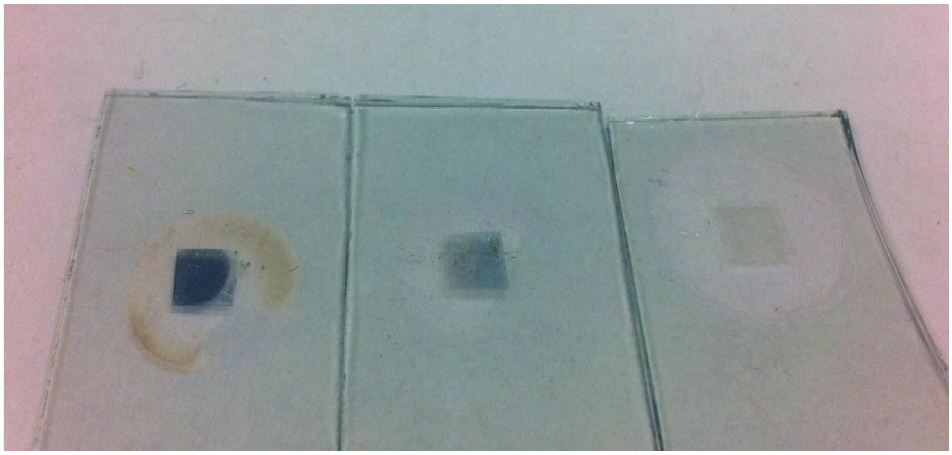

Figure 5.18: Optical response of sample IIIR to CA technique under applying -1 V (left), -0.5 V (middle) and +0.5 V (right)

To evaluate the coloration efficiency (CE) we used the conventional expression relating the efficiency with the optical density [73]. The calculated coloration efficiencies and their corresponding time responses are summarized in Table 5.2

	Coloring		Bleaching	
Sample ID	CE (cm^2C^{-1})	t (s)	CE (cm^2C^{-1})	t (s)
IR	6.02	24	20.39	0.6
IIR	7.03	19	21.15	1.4
IIIR	8.85	19	19.71	2.0
IVR	13.67	21	20.75	2.2
I250	17.61	19	5.52	4.3
I500	20.08	24	7.10	24

Table 5.2: Coloration efficiency, CE, and response time, t, during coloring and bleaching process. CE obtained from λ_{max} and response time is the time needed for the sample to reach 90% of ΔT_{max}

For non-annealed samples, both coloration efficiency and response time exhibit better performance during the bleaching process. The enhanced response time is lower than the recent reports for WO_3 nanostructured films and can be compared to the ultrafast

electrochromic devices [74] and those prepared by sol-gel technique [75]. Unlikely for annealed samples, coloration efficiency represents higher values for coloration process. However, the response time is always longer than bleaching in almost all samples. The coloration efficiencies in these devices are fairly good and comparable with those doped with gold [76] (but lower than those prepared with the doctor blade technique [12] [13]) and can be considered as characteristic of a moderately efficient electrochromic device. As seen earlier, the thickness of films was the order of tens of micrometer. High-thickness would generally result in lower coloration efficiency and longer switching response time. Nevertheless, electrochromic performance of films in this study exhibited fairly good functionality.

5.3 Diffusion Behaviour of Hydrogen Intercalation in Tungsten Oxide

The diffusion coefficient is a key parameter in modeling the electrochromic devices performing in an aqueous electrolyte and is basically obtained by various techniques such as Cyclic Voltammetry (CV), Chronocoulometry (CC), Galvanostatic Intermittent Titration Technique (GITT) [77] and Electrochemical Impedance Spectroscopy (EIS) [78]. In the context of our work, the first two techniques were used.

Cyclic Voltammetry (CV)

Due to Randles-Sevcik equation, in a diffusion-controlled CV measurement [79] the anodic peak is proportional to the square root of scan rate. A simplified form of the Randles-Sevcik equation at room temperature is:

$$i_p \approx 2.7 \times 10^5 \times n^{3/2} \times A \times D^{1/2} \times C_0 \times \nu^{1/2} \quad (5.2)$$

where i_p is the current peak, n=1 is the number of electrons involved in the process, A is the electrode area (cm^2), D (cm^2s^{-1}) is the diffusion coefficient, C_0 (mol/cm^3) is the solution concentration and ν (Vs^{-1}) is the scan rate.

It has been already reported that for a credible measurement of diffusion coefficient values obtained from CV peaks with the use of the Randles-Sevcik method, low scan rates are required [80]. This is mainly because slower rates of cycling will allow more time for the ions to be inserted into the EC films [80].The calculated diffusion coefficients are listed in Table 5.3 for different samples. It can be seen that the diffusion behaviour of the films decreases as the amount of particles increases. It has also been reported that annealing at 500°C decreases the value of the diffusion coefficient by an order of magnitude [81]. The overall order of magnitude of diffusion coefficients for the samples is seen to be rather high compared to the reports from other techniques (see for example those prepared by sol-gel [82][83], sputtering and thermal evaporation [28]). Fast proton kinetics in this study is responsible for the small delay in coloration as discussed in section 5.3.

Sample ID	D $\times 10^{-6}(cm^2s^{-1})$
IR	11.7
IIR	12.0
IIIR	9.02
IVR	5.62
I250	14.8
I500	2.29

Table 5.3: Diffusion coefficient values obtained by Randles-Sevcik equation

Moreover, the cathodic current peak in all CV measurements is always higher than the anodic current peak which reflects the fact that diffusion during the bleaching reaction is faster than that of the coloration and is in agreement with the rapid decay of current during bleaching.

Chronocoulometry (CC)

Anson [84] showed that in a well-behaved electrochemical system, the inserted (extracted) charge is proportional to $t^{1/2}$ and the system acts like a capacitor charging (discharging) during each segment. As can be seen from Figure 5.15 'b', the only CC patterns that obey Anson's law are those working under applied voltages lower than -0.8 V. On the other hand, for potentials -0.8 V and above we can observe such behaviour only for the first couple of seconds in the beginning of the experiment and thereafter CC patterns tend to have a linear relationship with time. The same behaviour can be also observed for the bleaching process. This implies that there is a critical potential point at which the system alters its diffusion behaviour to a non-diffusion one. At potentials above this critical point the charges are irreversibly trapped until the applied potential polarity is reversed. As concluded earlier, not all of these inserted charges are involved in the coloring process. One of the main issues for film degradation is the film being subject to a certain range of potential and, therefore, choice of the applied potential has to be taken under consideration.

5.4 Electronic Properties of Tungsten Oxide to Tungsten Bronze Transition

Generally speaking, the applied potential can be described as:

$$E = E_{i=0} + ASR.J_{(t)} + \eta_{(t)} \quad (5.3)$$

where $E_{i=0}$ is the open-circuit potential (versus reference electrode) of WO_3, $ASR.J_{(t)}$ is the voltage drop across the WO_3/electrolyte interface in which the electrochemical reaction is controlled by the area specific resistance ASR. The overpotential, $\eta_{(t)}$, which is the driving force, is responsible for the electrochemical reaction at the WO_3/ electrolyte interface. According to the Butler-Volmer relationship [85], $\eta_{(t)}$ varies linearly with log $J_{(t)}$. The origin of the ohmic behaviour depends highly on the conductivity of the electrolyte, the structure and thickness of the films and the conductivity of electronic substrate layer and can be therefore expressed as the sum of the following series resistances:

$$R = R\,(\text{electrolyte}) + R\,(H_iWO_3) + R\,(\text{ITO}) + R\,(\text{ITO}/H_iWO_3) \quad (5.4)$$

Figure 5.19 ‘a’ represents the current densities extracted from Figure 5.15 during the coloration (middle segment). Its corresponding optical density (OD) is plotted in Figure 19 ‘b’ for the wavelength 650 nm.

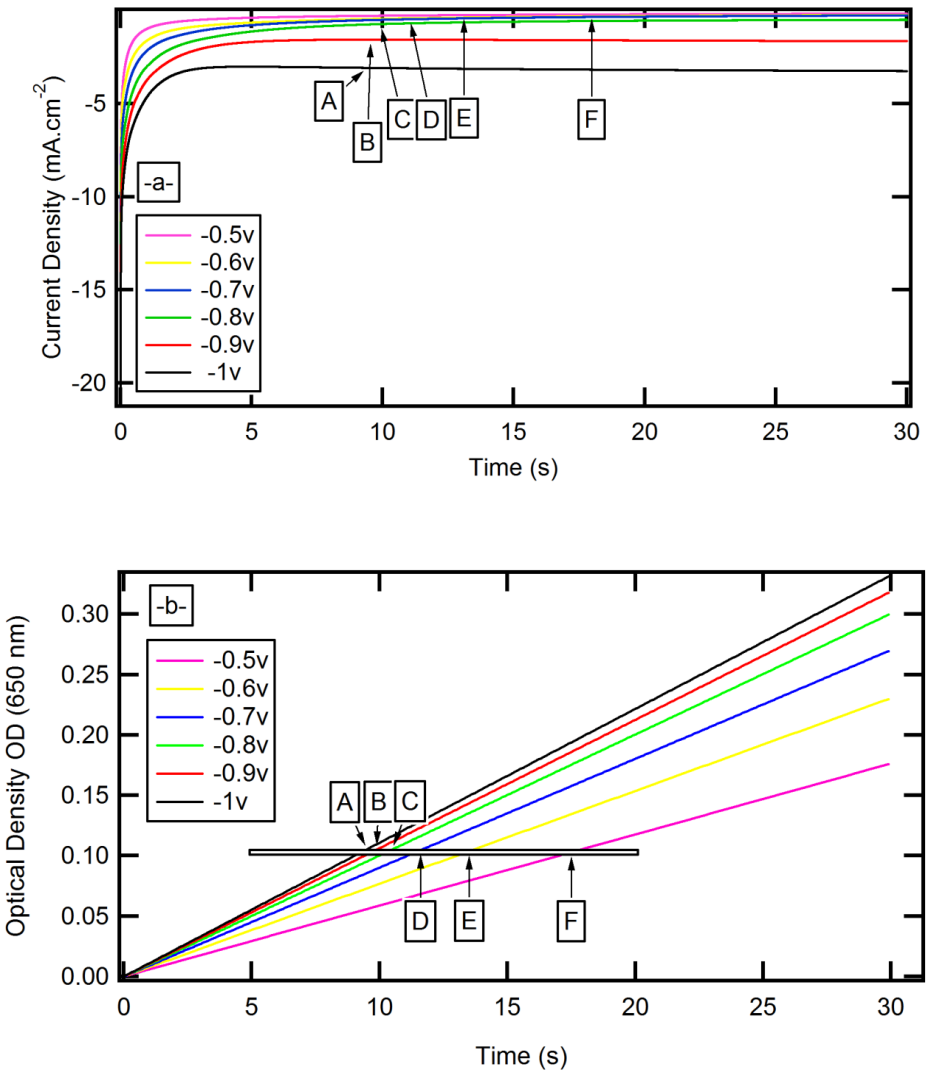

Figure 5.19: Current density during coloring reaction in CA technique, a, and the optical response, b

If we assume that the inserted amount of charge into the films (x) at one point is equal to "i" we can then say that the films have a non-stoichiometric form of a H_iWO_3 at the point which is responsible for the appearing color (OD_i). Apparently, two identical bronze forms H_iWO_3 and H_jWO_3 have the same color and electrochemical behaviours if and only if i = j. Thus if an imaginary line which is parallel to the horizontal axis intersects with the curves in Figure 5.19 'b', the points of intersection should have the same amount of

OD and therefore should refer to same form of bronze. As an example, for OD = 0.1 this imaginary line intersects with the curves at points A, B, C, D, E and F which are shown on Figure 5.19 'b'. Each takes place at a specific time and we can therefore obtain their current densities from Figure 5.19 'a'. We are now able to plot the current densities versus applied potentials for OD=1. The same was done for OD = 0.1 and 0.15 as shown in Figure 5.20.

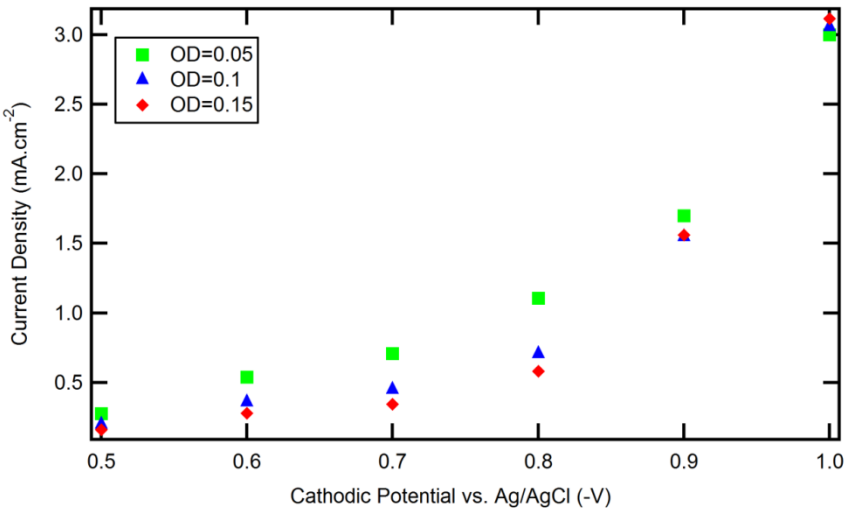

Figure 5.20: Current density versus applied potential in CA technique obtained for different optical densities

For potentials below -0.8 V each OD represents a linear ohmic behaviour. For a constant potential, the current densities are shifted lower as OD increases which is due to the shift in the open-circuit potential ($E_{i=0}$). $E_{i=0}$ becomes more negative as the ion insertion proceeds in the films [86]. Following the approach from Vuillemin and Bohnke in which they assumed that $\eta_{(t)} << ASR.J_{(t)}$ at the beginning of the coloration [70] and by linear fitting and inverting for the curve OD = 0.05 (that satisfies the assumption) we obtained the value for the area specific resistance ASR = 463.3 Ωcm^2. Compared to the 91 Ωcm^2

for the WO_3 films prepared by thermal evaporation performed in sulphuric acid [70], the area specific resistance in this study is higher. This is mainly due to the high thickness of the films that can affect the conductivity dramatically.

5.5 Factors Contributing to the Instability of the Device

The main reason that causes deterioration of the sample (non-annealed samples, in particular) would be the solubility of tungsten oxide in acidic electrolyte rather than electrochemical barriers. Although tungsten oxide exhibit very good electrochemical properties in sulphuric acid, this unwanted solubility has been already reported to be an issue for devices based on tungsten oxide [87].

It has also been observed that the conductivity of ITO diminishes after some period of time in sulphuric acid. We measured the resistance of ITO while the sample is indicating good electrochemical behaviour and we found out that the ITO layer has a higher resistance compared to the unused one. Films that showed poor electrochemical activity in the electrochemical cell were also measured in the same manner. While they did not show any corrosion of the tungsten oxide films, the part of ITO in contact with sulphuric acid indicates high resistance (insulating behaviour). This is mainly because ITO thickness decreases when in contact with an acidic media, giving rise to a higher resistance of the layer [88].

Beside those systematic problems, the application of an excessive potential can easily damage the films. As discussed in section 5.3, these potentials can cause an unusual

electrochemical and electrochromic behaviour. If the sample is kept continuously under the same conditions, the gradual irreversible reactions weaken the electrochemical patterns.

6. Conclusion

For the first time, nanostructured tungsten oxide films were prepared from tungsten oxide nanoparticles by the filtration and transfer method onto ITO-coated glass substrates. This method is proven to be versatile, representing many advantages. The thinnest films are generally a mixture of sparse and scattered tungsten oxide nanoparticles. The surface coverage increases with further agglomeration of particles. Aggregates ranging from 100 to 300 nm can be clearly seen in the SEM images for all samples. Smaller size aggregates were observed in samples prepared from suspensions with a lower amount of tungsten oxide nanoparticles. The lower surface coverage characterizing these samples led to higher pore size films. The thickness of the films was found to be depending on preparation conditions and, in particular, on the amount of nanoparticles in the suspensions. These films are practically thicker than the nanostructured films prepared via other techniques. After annealing at 250 and 500^{o}C, the particles become highly packed together resulting in the formation of aggregates ranging from 3 to 10 μm. One can see from higher-magnification SEM images that the cores of these aggregates are constituted by tungsten oxide nanoparticles with an average size of 50 nm. An increase in the crystallinity of the films would be expected by further increasing the annealing temperature from 250 to 500^{o}C. For very dense samples, the films showed a more uniform appearance.

Cyclic voltammetry has shown that the diffusion of the ions injected into the films is fast, which is a measure of the kinetics of the electrode reaction. At low scan rates the reactions at the surface of the electrode occur in an almost steady state manner, requiring

more time for each cycle and resulting in a higher optical modulation. For annealed samples, the current density decreases after the 350^{th} cycle. The durability of the films, however, is lower for non-annealed ones. This is in agreement with the reported conclusion that a high degree of crystallization leads to an improvement the electrochromic lifetime.

On the other hand, the current density peak for the bleaching process during chronoamperometry is higher than that for coloration and the current density during bleaching decays faster than for the coloration process. The former is a consequence of high conductivity of the HWO_3 bronze and the latter is due to the HWO_3 -WO_3 transition. This behaviour was seen when we observed the fast switching response time during the bleaching process. This value for some samples was of the order of a second which is lower than indicated by the recent reports for WO_3 nanostructured films and can be compared to the ultrafast electrochromic devices [74] and those prepared by sol-gel technique [75]. The coloration efficiency for this device was about 20 cm^2C^{-1}.

For both techniques mentioned above, the coloration of the films is associated with the number of color centers and depends on the number of inserted charges. Nevertheless, the optical reversibility has always a higher value than the charge reversibility disregarding applied potential and this is mainly because the inserted charges that stay in the trap sites during the bleaching are not involved in the coloration process.

Results from this thesis by all means are not definite. The nanosized electrochromic films prepared in this way can be certainly optimized in terms of electrochromic properties and performance.

Although tungsten oxide performs very well in acidic solutions like sulphuric acid, this is one of the main issues for deterioration of the electrochromic layer on the substrates. Using a gel electrolyte can lead to an increase of the interfacial adhesion of the nanostructured WO_3/ITO interfaces and can affect the durability of the device by preventing the electrochromic layer from dissolving into the acid.

Mixed nanostructured electrochromic devices have already been shown to enhance device performance and lifetime. For future studies, it would be interesting to investigate if other electrochromic nanoparticles, such as TiO_2 or MoO_3 nanoparticles, could be mixed with WO_3 nanoparticles in order to achieve higher optical contrast and coloration efficiency. Our preparation method for nanoparticles thin films, the filtration and transfer method, would be an excellent method for devising such films. The variables involved include the nanoparticle size and concentration, as well as the type of the electrochromic material. In fact, more than two electrochromic materials can also be envisaged.

Our final suggestion would be a method for enhancing the switching time. Electrochromic materials can be deposited on a nanowire template (e.g., a zinc oxide template). Such a zinc oxide nanowire electrode-based EC display has the potential to exhibit fast response times due to the large surface area involved and good electron transport properties of the nanowires.

References

1. M. Ferrara, and M. Bengisu, *Materials that Change Color: Smart Materials*, *Intelligent Design*, Springer (2013).

2. S.-H. Lee, R. Deshpande, P.A. Parilla, K.M. Jones, B. To, A.H. Mahan, and A.C. Dillon, *Crystalline WO_3 nanoparticles for highly improved electrochromic applications*, Advanced Materials 18, 763 (2006).

3. *Raising the IQ of smart windows*, http://newscenter.lbl.gov/news-releases/2013/08/14/raising-the-iq-of-smart-windows/, [Online] August 04, 2013.

4. C.M. Lampert, *Large-area smart glass and integrated photovoltaics*, Solar Energy Materials and Solar Cells 76, 489 (2003).

5. C.M. Lampert, *Electrochromics-history, current status and potential*, Glass Science and Technology 75, 244 (2002).

6. M. Green, and K. Pita, *Non-stoichiometry in thin film dilute tungsten bronzes: M_xWO_y*, Solar Energy Materials and Solar Cells 43, 393 (1996).

7. S.-H. Lee, H.M. Cheong, P. Liu, D. Smith, C. E. Tracy, A. Mascanrenhas, J. R. Pitts, and S.K. Deb, *Gasochromic mechanism in a-WO_3 thin films based on Raman spectroscopic studies*, Journal of Applied Physics 88, 3076 (2000).

8. C.G. Granqvist, *Electrochromic tungsten oxide films: review of progress 1993–1998*, Solar Energy Materials and Solar Cells 60, 201 (2000).

9. C.G. Granqvist, *Handbook of inorganic electrochromic materials*, Elsevier (1995).

10. C.G. Granqvist, *Oxide electrochromics: an introduction to devices and materials*, Solar Energy Materials and Solar Cells 99, 1 (2012).

11. R.J. Mortimer, *Electrochromic materials*, Annual Review of Materials Research 41, 241 (2011).

12. N.N. Dinh, D.H. Ninh, T.T. Thao, and V.-V Truong, *Mixed nanostructured Ti-W oxides films for efficient electrochromic windows*, Journal of Nanomaterials 781236, 1 (2012).

13. N.N. Dinh, N.M. Quyen, D.N. Chung, M. Zikova, and V.-V. Truong, *Highly-efficient electrochromic performance of nanostructured TiO_2 films made by doctor blade technique*, Solar Energy Materials and Solar Cells 95, 618 (2011).

14. C. Costa, C. Pinheiro, I. Henriques, and C.A.T. Laia, *Inkjet printing of sol–gel synthesized hydrated tungsten oxide nanoparticles for flexible electrochromic devices*, ACS Applied Materials and Interfaces 4, 1330 (2012).

15. J. Luo, Q. Zeng, Y. Long, and Y. Wang, *Preparation of nano-polycrystalline WO_3 thin films and their solid-state electrochromic display devices*, Journal of Nanoscience and Nanotechnology 13, 1372 (2013).

16. S. Badilescu, and P.V. Ashrit, *Study of sol–gel prepared nanostructured WO_3 thin films and composites for electrochromic applications*, Solid State Ionics 158, 187 (2003).

17. S.K. Deb, *Optical and photoelectric properties and colour centres in thin films of tungsten oxide*, Philosophical Magazine 27, 801 (1973).

18. C. Bechinger, S. Ferrere, A. Zaban, J. Sprague, and B.A. Gregg, *Photoelectrochromic windows and displays*, Nature 383, 608 (1996).

19. S.-H. Lee, H.M. Cheong, J.-G. Zhang, A. Mascarenhas, D. K. Benson, and S.K. Deb, *Electrochromic mechanism in a-WO_{3-y} thin films*, Applied Physics Letters 74, 242 (1999).

20. M. Gratzel, *Photoelectrochemical cells*, Nature 414, 338 (2001).

21. M. Wagemaker, A.P. M. Kentgens, and F. M. Mulder, *Equilibrium lithium transport between nanocrystalline phases in intercalated TiO_2 anatase*, Nature 418, 397 (2002).

22. Z.C. Wu, Z.H. Chen, X. Du, J.M. Logan, J. Sippel, M. Nikolou, K. Kamaras et al., *Transparent conductive carbon nanotubes films*, Science 305, 1273 (2004).

23. E. Bica, E.J. Popovici, M. Stefan, I. Perhaita, L. Barbu-Tudoran, E. Indrea, and I.C. Popescu, *Morphological, structural and optical characterization of tungsten trioxide films prepared by sol-gel route: effect of substrate and annealing temperature*, Digest Journal of Nanomaterials and Biostructures 6,1935 (2011).

24. N.M. Rowley, and R.J. Mortimer, *New electrochromic materials*, Science Progress 85, 243 (2002).

25. P.M. Beaujuge, and J.R. Reynolds, *Color control in π-conjugated organic polymers for use in electrochromic devices*, Chemical Reviews 110, 268 (2010).

26. R.D. Rauh, *Electrochromic windows: an overview*, Electrochimica Acta 44, 3165 (1999).

27. I.F. Chang, B.L. Gilbert, and T.I. Sun, *Electrochemichromic systems for display applications*, Journal of The Electrochemical Society 122, 955 (1975).

28. P.M.S. Monk, R.J. Mortimer, and D.R. Rosseinsky, *Electrochromism and electrochromic devices,* Cambridge University Press (2007).

29.P. Somani, and S. Radhakrishnan*, Charge transport processes in conducting polypyrrole/Prussian Blue bilayers*, Materials Chemistry and Physics 76, 15 (2002).

30. R.J. Mortimer, *Organic electrochromic materials*, Electrochimica Acta 44, 2971 (1999).

31. G.A. Niklasson, and C.G. Granqvist, *Electrochromics for smart windows: thin films of tungsten oxide and nickel oxide, and devices based on these*, Journal of Materials Chemistry 17, 127 (2007).

32. R.G. Goodchild, J.B. Webb, and D.F. Williams, *Electrical properties of highly conducting and transparent thin films of magnetron sputtered* SnO_2, Journal of Applied Physics 57, 2308 (1985).

33. C.M. Lampert, *Electrochromic materials and devices for energy efficient windows*, Solar Energy Materials 11, 1 (1984).

34. C.F. Klingshirn, *Semiconductor optics*, Springer (2007).

35. W. Sahle, and M. Nygren, *Electrical conductivity and high resolution electron microscopy studies of* WO_{3-x} *crystals with* $0 \leq x \leq 0.28$, Journal of Solid State Chemistry 48, 154 (1983).

36. B. Ingham, S.C. Hendy, S.V. Chong, and J.L. Tallon, *Density-functional studies of tungsten trioxide, tungsten bronzes, and related systems*, Physical Review B 72, 075109 (2005).

37. P.J. Wiseman, and P.G. Dickens, *Neutron diffraction studies of cubic tungsten bronzes*, Journal of Solid State Chemistry 17, 91 (1976).

38. R. Clarke, *New sequence of structural phase transitions in $NaxWO_3$*, Physical Review Letters 39, 1550 (1977).

39. B.W. Brown, and E. Banks, *The sodium tungsten bronzes*[1,2], Journal of the American Chemical Society 76, 963 (1954).

40. A. Hjelm, C.G. Granqvist, and J.M. Wills, *Electronic structure and optical properties of WO_3, $LiWO_3$, $NaWO_3$, and HWO_3*, Physical Review B 54, 2436 (1996).

41. C.G. Granqvist, A. Azens, J. Isidorsson, M. Kharrazi, L. Kullman, T. Lindström, G. A. Niklasson et al., *Towards the smart window: progress in electrochromics*, Journal of Non-Crystlline Solids 218, 273 (1997).

42. M. Figlarz, *New oxides in the WO_3-MoO_3 system*, Progress in Solid State Chemistry 19, 1 (1989).

43. P.J. Wiseman, and P.G. Dickens, *The crystal structure of cubic hydrogen tungsten bronze*, Journal of Solid State Chemistry 6, 374 (1973).

44. J. Shim, C.-R. Lee, H.-K. Lee, J.-S. Lee, and E.J. Cairns, *Electrochemical characteristics of Pt–WO_3/C and Pt–TiO_2/C electrocatalysts in a polymer electrolyte fuel cell*, Journal of Power Sources 102, 172 (2001).

45. P.J. Kulesza, and L.R. Faulkner, *Electrocatalysis at a novel electrode coating of nonstoichiometric tungsten (VI, V) oxide aggregates*, Journal of the American Chemical Society 110, 4905 (1988).

46. P. Schlotter, and L. Pickelmann, *The xerogel structure of thermally evaporated tungsten oxide layers*, Journal of Electronic Materials 11, 207 (1982).

47. N. Yoshiike, and S. Kondo, *Behavior of a-WO_3 film in propylene carbonate electrolytes*, Denki Kagaku 54, 423 (1986).

48. B.W. Faughnan, *Electrochromism in WO_3 amorphous films*, RCA Review 36, 177 (1975).

49. R.S. Crandall, and B.W. Faughnan, *Measurement of the diffusion coefficient of electrons in WO_3 films*, Applied Physics Letters 26, 120 (1975).

50. S. Arman, *Electrochromic materials for display applications: An introduction*, Journal of New Materials for Electrochemical Systems 4, 173 (2001).

51. S.K. Deb, *A novel electrophotographic system*, Applied Optics 8, 192 (1969).

52. F.A. Settle, *Handbook of instrumental techniques foranalytical chemistry*, Prentice Hall (1997).

53. D. Pletcher, *A first course in electrode processes*, Electrochemical Consultancy (1991).

54. Model 600 series electrochemical analyzer user manual, *CH Instruments Inc.*

55. D. Vernardou, H. Drosos, E. Spanakis, E. Koudoumas, C. Savvakis, and N. Katsarakis, *Electrochemical and Photocatalytic Properties of WO_3 Coatings Grown at Low Temperatures*, Journal of Materials Chemistry 21, 513 (2011).

56. Y. Djaoued, S. Balaji, and R. Brüning, *Electrochromic devices based on porous tungsten oxide thin films*, Journal of Nanomaterials 7, 674168 (2012).

57. N.N. Dinh, N.Th.T. Oanh, P.D. Long, M.C. Bernard, and A. H.-L. Goff, *Electrochromic properties of TiO_2 anatase thin films prepared by a dipping sol–gel method*, Thin Solid Films. 423, 70 (2003).

58. S.J.Yoo, J.W. Lim, Y.-E. Sung, Y.H. Jung, H.G. Choi, and D.K. Kim, *Fast switchable electrochromic properties of tungsten oxide nanowire bundles*, Applied Physics Letters 90, 173126 (2007).

59. H. Zheng, J. Z. Ou, M.S. Strano, R.B. Kaner, A. Mitchell, and K. Kalantar-zadeh, *Nanostructured tungsten oxide–properties, synthesis, and applications*, Advanced Functional Materials 21, 2175 (2011).

60. J.P. Cronin, S.R. Kennedy, A. Agrawal, T.J. Gudgel, Y.J. Yao, J.C.L. Tonazi, and D.R. Uhlmann, *Electrochemistry of glasses and ceramics*, Ceramic Transactions 92, 175 (1999).

61. M. Deepa, T.K. Saxena, D.P. Singh, K.N. Sood, and S.A. Agnihotry, *Spin coated versus dip coated electrochromic tungsten oxide films: structure, morphology*, *optical and electrochemical properties,* Electrochimica Acta 51, 1974 (2006).

62. M. Deepa, M. Kar, and S.A. Agnihotry, *Electrodeposited tungsten oxide films: annealing effects on structure and electrochromic performance*, Thin Solid Films 468, 32 (2004).

63. A.G. Souza-Filho, V.N. Freire, J.M. Sasaki, J. Mendes Filho, J.F. Juliao, and U.U. Gomes, *Coexistence of triclinic and monoclinic phases in WO_3 ceramics*, Journal of Raman Spectroscopy 31, 451 (2000).

64. S. Panero, B. Scrosati, M. Baret, B. Cecchini, and E. Masetti, *Electrochromic windows based on polyaniline, tungsten oxide and gel electrolytes*, Solar Energy Materials and Solar Cells 39, 239 (1995).

65. C. Marcel, M.S. Hegde, A. Rougier, C. Maugy, C. Guéry, and J-M. Tarascon, *Electrochromic properties of antimony tin oxide (ATO) thin films synthesized by pulsed laser deposition*, Electrochimica Acta 46, 2097 (2001).

66. D.-J. Kim, and S.-I. Pyun, *Hydrogen transport through rf-magnetron sputtered amorphous WO_3 film with three kinds of hydrogen injection sites*, Solid State Ionics 99, 185 (1997).

67. N.M. Vuong, D. Kim, and H. Kim, *Electrochromic properties of porous WO_3 –TiO_2 core–shell nanowires*, Journal of Materials Chemistry C 1, 3399 (2013).

68. X. Chang, S. Sun, Z. Li, X. Xu, and Y. Qiu, *Assembly of tungsten oxide nanobundles and their electrochromic properties*, Applied Surface Science 257, 5726 (2011).

69. A. Enesca, A. Duta, L. Isac, S. Manolache, and J. Schoonman, *The influence of the annealing process on the properties of WO_3 photoelectrode used in a photoeletrochemical cell (PECC)*, In Journal of Physics: Conference Series 61, 472 (2007).

70. B. Vuillemin, and O. Bohnke, *Kinetics study and modelling of the electrochromic phenomenon in amorphous tungsten trioxide thin films in acid and lithium electrolytes*, Solid State Ionics 68, 257 (1994).

71. K.D. Lee, *Influence of film thickness on the chemical stability of electrochromic tungsten oxide film*, Journal of the Korean Physical Society 38, 33 (2001).

72. H. Wang, X. Quan, Y. Zhang, and S. Chen, *Direct growth and photoelectrochemical properties of tungsten oxide nanobelt arrays*, Nanotechnology 19, 065704 (2008).

73. Z. Jiao, J. Wang, L. Ke, X. Liu, H.V. Demir, M.F. Yang, and X.W. Sun, *Electrochromic properties of nanostructured tungsten trioxide (hydrate) films and their applications in a complementary electrochromic device*, Electrochimica Acta 63, 153 (2012).

74. Z. Jiao, X. Wang, J. Wang, L. Ke, H.V. Demeir, T.W. Koh, and X.W. Sun, *Efficient synthesis of plate-like crystalline hydrated tungsten trioxide thin films with highly improved electrochromic performance*, Chemical Communications 48, 365 (2012).

75. L. Yang, D. Ge, J. Zhao, Y. Ding, X. Kong, and Y. Li, *Improved electrochromic performance of ordered macroporous tungsten oxide films for IR electrochromic device*, Solar Energy Materials and Solar Cells 100, 251 (2012).

76. N. Naseri, R. Azimirad, O. Akhavan, and A. Z. Moshfegh, *Improved electrochromical properties of sol–gel WO_3 thin films by doping gold nanocrystals*, Thin Solid Films 518, 2250 (2010).

77. M. Giannouli, and G. Leftheriotis, *The effect of precursor aging on the morphology and electrochromic performance of electrodeposited tungsten oxide films*, Solar Energy Materials and Solar Cells 95, 1932 (2011).

78. S.-H. Lee, H.M. Cheong, C. E. Tracy, A. Mascarenhas, R. Pitts, G. Jorgensen, and S.K. Deb, *Influence of microstructure on the chemical diffusion of lithium ions in amorphous lithiated tungsten oxide films*, Electrochimica Acta 46, 3415 (2001).

79. I. Shiyanovskaya, M. Hepel, and E. Tewksburry, *Electrochromism in electrodeposited nanocrystalline WO_3 films I. Electrochemical and optical properties*, Journal of New Materials for Electrochemical Systems 3, 241 (2000).

80. G. Leftheriotis, S. Papaefthimiou, and P. Yianoulis, *Dependence of the estimated diffusion coefficient of Li_xWO_3 films on the scan rate of cyclic voltammetry experiments*, Solid State Ionics 178, 259 (2007).

81. M. Deepa, A.K. Srivastava, T.K. Saxena, and S.A. Agnihotry, *Annealing induced microstructural evolution of electrodeposited electrochromic tungsten oxide films*, Applied Surface Science 252, 1568 (2005).

82. M. Deepa, P. Singh, S.N. Sharma, and S.A. Agnihotry, *Effect of humidity on structure and electrochromic properties of sol–gel-derived tungsten oxide films*, Solar Energy Materials and Solar Cells 90, 2665 (2006).

83. M. Alsawafta, Y. Mosaddeghian Golestani, T. Phonemac, S. Badilescu, V. Stoncovski, and Vo-Van Truong, *Electrochromic Properties of Sol-Gel Synthesized*

Macroporous Tungsten Oxide Films Doped with Gold Nanoparticles, Journal of The Electrochemical Society 161, 276 (2014).

84. F.C. Anson, and R.A. Osteryoung, *Chronocoulometry: A convenient, rapid and reliable technique for detection and determination of adsorbed reactants*, Journal of Chemical Education 60, 293 (1983).

85. J.O'M. Bockris, and A.K.N. Reddy, *Modern Electrochemistry,* Plenum Press (1970).

86. T. Kamimori, J. Nagai, and M. Mizuhashi, *Transport of Li^+ ions in amorphous tungsten oxide films*, 27th Annual Techincal Symposium pp. 51-56, International Society for Optics and Photonics (1983).

87. W. Cheng, E. Baudrin, B. Dunn, and J.I. Zink, *Synthesis and electrochromic properties of mesoporous tungsten oxide*, Journal of Materials Chemistry 11, 92 (2001).

88. G. Wantz, L. Hirsch, N. Huby, L. Vignau, J.F. Silvain, A.S. Barriére, and J.P. Parneix, *Correlation between the indium tin oxide morphology and the performances of polymer light-emitting diodes*, Thin Solid Films 485, 247 (2005).